SANDIA REPORT
SAND2006-7729
Unlimited Release
Printed December 2006

SAR Processing with Non-Linear FM Chirp Waveforms

Armin W. Doerry

Prepared by
Sandia National Laboratories
Albuquerque, New Mexico 87185 and Livermore, California 94550

Sandia is a multiprogram laboratory operated by Sandia Corporation,
a Lockheed Martin Company, for the United States Department of Energy's
National Nuclear Security Administration under Contract DE-AC04-94AL85000.

Approved for public release; further dissemination unlimited.

Sandia National Laboratories

Issued by Sandia National Laboratories, operated for the United States Department of Energy by Sandia Corporation.

NOTICE: This report was prepared as an account of work sponsored by an agency of the United States Government. Neither the United States Government, nor any agency thereof, nor any of their employees, nor any of their contractors, subcontractors, or their employees, make any warranty, express or implied, or assume any legal liability or responsibility for the accuracy, completeness, or usefulness of any information, apparatus, product, or process disclosed, or represent that its use would not infringe privately owned rights. Reference herein to any specific commercial product, process, or service by trade name, trademark, manufacturer, or otherwise, does not necessarily constitute or imply its endorsement, recommendation, or favoring by the United States Government, any agency thereof, or any of their contractors or subcontractors. The views and opinions expressed herein do not necessarily state or reflect those of the United States Government, any agency thereof, or any of their contractors.

Printed in the United States of America. This report has been reproduced directly from the best available copy.

Available to DOE and DOE contractors from
U.S. Department of Energy
Office of Scientific and Technical Information
P.O. Box 62
Oak Ridge, TN 37831

Telephone: (865) 576-8401
Facsimile: (865) 576-5728
E-Mail: reports@adonis.osti.gov
Online ordering: http://www.osti.gov/bridge

Available to the public from
U.S. Department of Commerce
National Technical Information Service
5285 Port Royal Rd.
Springfield, VA 22161

Telephone: (800) 553-6847
Facsimile: (703) 605-6900
E-Mail: orders@ntis.fedworld.gov
Online order: http://www.ntis.gov/help/ordermethods.asp?loc=7-4-0#online

SAND2006-7729
Unlimited Release
Printed December 2006

SAR Processing with Non-Linear FM Chirp Waveforms

Armin W. Doerry
SAR Applications Department

Sandia National Laboratories
PO Box 5800
Albuquerque, NM 87185-1330

ABSTRACT

Nonlinear FM (NLFM) waveforms offer a radar matched filter output with inherently low range sidelobes. This yields a 1-2 dB advantage in Signal-to-Noise Ratio over the output of a Linear FM (LFM) waveform with equivalent sidelobe filtering.

This report presents details of processing NLFM waveforms in both range and Doppler dimensions, with special emphasis on compensating intra-pulse Doppler, often cited as a weakness of NLFM waveforms.

ACKNOWLEDGEMENTS

This work was funded by the US DOE Office of Nonproliferation & National Security, Office of Research and Development, NA-22, under the Advanced Radar System (ARS) project.

Sandia is a multiprogram laboratory operated by Sandia Corporation, a Lockheed Martin Company, for the United States Department of Energy under Contract DE-AC04-94AL85000.

CONTENTS

FOREWORD 6
1 Introduction & Background 7
2 Overview & Summary 9
3 Basic Principles 11
3.1 The Received Echo from a Single Pulse 11
3.2 Radar Ambiguity Function 13
3.3 Pulse Compression 16
3.4 Multiple Pulses 17
3.5 Geometry Details 18
3.6 Intra-Pulse Doppler – When is it Significant? 21
4 Simple Range and Doppler Measurements 25
4.1 Time-Domain Processing – Negligible Intra-Pulse Doppler 26
4.2 Frequency-Domain Processing – Negligible Intra-Pulse Doppler 29
4.3 Compensating Intra-Pulse Doppler 32
4.4 Compensating Intra-Pulse Doppler – Method 2 35
4.5 Compensating Intra-Pulse Doppler – Method 3 39
4.6 So What's the Point? 44
5 SAR Processing 45
5.1 SAR Processing – Negligible Intra-Pulse Doppler 45
5.2 SAR Processing – Uniform Intra-Pulse Doppler 50
5.3 SAR Processing – Intra-Pulse Doppler Variations 54
5.4 Stretch Processing 60
5.5 So What's the Point? 60
6 Conclusions 61
REFERENCES 63
DISTRIBUTION 66

FOREWORD

Often, especially for power-starved radar systems, the radar designer strives to extract every bit of performance that he is able to coax from his system. A single dB of additional Signal-to-Noise Ratio (SNR) gained elsewhere is equivalent to a 25% increase in transmitter power. Alternatively, a single dB of additional SNR can have dramatic effects in reducing false alarm rates in target detection applications.

Recently, Sandia has participated in system engineering efforts for several orbital SAR systems, where performance was indeed limited by achievable SNR. In spite of this, Linear FM (LFM) waveforms were selected, principally based on their familiarity to the system designers. Non-Linear FM (NLFM) waveforms were not considered, principally due to the lack of familiarity with them.

This spurred side efforts at Sandia to understand in greater detail the benefits and costs of using NLFM waveforms. An earlier report detailed designing and generating NLFM waveforms. This report details processing SAR images with them.

1 Introduction & Background

It is well known that when a signal is input to a Matched Filter (matched to the input signal) then the output of the filter is the autocorrelation function of the signal. Also well known is that the autocorrelation function is the Fourier Transform of the signal's Energy Spectral Density (ESD). A Matched Filter provides optimum (maximum) Signal to Noise Ratio (SNR) at the peak of its autocorrelation function, and is consequently optimum for detecting the signal in noise.

A very common radar waveform is the Linear FM (LFM) chirp signal. Its utility is that it is fairly readily generated by a variety of technologies, and is easily processed by a variety of techniques that ultimately implement a Matched Filter, or nearly so. However, since a LFM chirp waveform has nearly a rectangular ESD, its autocorrelation function exhibits a sinc() function shape, with its attendant problematic sidelobe structure.

Reducing the sidelobes of the Matched Filter output (actually increasing the peak to sidelobe ratio) is typically accomplished by linear filtering the output, most often by applying window functions or data tapering. This additional filtering perturbs the Matched Filter result to reduce sidelobes as desired. However, since the cumulative filtering is no longer precisely matched to the signal, it necessarily reduces output SNR as well, typically by 1-2 dB (depending on the filtering or weighting function used).[1]

It is well-known that Non-Linear FM (NLFM) chirp modulation can advantageously shape the ESD such that the autocorrelation function exhibits substantially reduced sidelobes from its LFM counterpart. Consequently, no additional filtering is required and maximum SNR performance is preserved, although this is strictly only true in the range direction of range-Doppler processing. However precision NLFM chirps are more difficult to design, produce, and process.

Alternatives to NLFM modulation for the purpose of shaping the PSD, such as amplitude tapering the transmitted signal, are not viable since typically efficient power amplification of the waveform necessitates operating the hardware in a nonlinear manner, e.g. operating the amplifiers in compression. This substantially reduces the ability to maintain precision amplitude tapering. Waveform phase remains unaffected by operating amplifiers in compression.

What is desired by a radar designer is then a NLFM waveform that is 1) easily designed to meet target performance criteria, including bandwidth constraints and sidelobe reduction goals, 2) easily generated, and 3) easily processed.

Prior reports detailed designing and generating precision NLFM waveforms.[2,3] The advent of modern high-speed processors allow more complex filtering and detection algorithms to be employed. What are needed to facilitate this are the algorithms that are easily implemented in these new processors. However, the unique characteristics of

NLFM waveforms also include unique problems in their processing for maximizing system performance.

Several papers suggest that an issue for NLFM waveforms is their tolerance to Doppler shifts, i.e., maintaining their desirable sidelobe properties when Doppler shifted by relative motion between radar and target. The literature suggests this to be of particular concern to weather radars.

Keel, et al.,[4] describe the problem of waveform Doppler intolerance, and propose a "nonlinear step frequency waveform which is derived from sampling a Dolph-Chebyshev weighting function." They offer no mitigation scheme other than designing a waveform that doesn't suffer too badly. Johnston[5] analyzes the effect of Doppler shift on NLFM signals, but offers no mitigation schemes. Keeler and Hwang[6] analyze and compare several modulation schemes for their Doppler tolerance. Their application is weather radar with relatively small time-bandwidth products (<100), compared to high-performance Synthetic Aperture Radar (SAR).

Griffiths and Vinagre,[7] in describing a particular NLFM waveform they have designed, go out of their way to state "When the full ambiguity function of this type of waveform is evaluated it is found that its Doppler tolerance is excellent, giving essentially the same peak sidelobe level over the whole of the Doppler bandwidth corresponding to the antenna footprint." This is clearly a concern for NLFM waveforms.

Morgan[8] proposes a hybrid approach using a NLFM waveform along with employing window functions to trade Doppler tolerance for SNR gain. This was also analyzed by Collins and Atkins[9] for sonar applications. However Johnston and Fairhead[10] state "the choice of window function [i.e. desired ESD taper for NLFM design] appears less important than previously supposed, although the truncated Gaussian window does give slightly better tolerance than the others to Doppler shift."

Rihaczek[11] differentiates between Doppler-invariant and Doppler-tolerant waveforms, and discusses a class of waveforms where only some aspects of the waveform are Doppler-invariant.

Urkowitz and Bucci[12] describe a filtering technique to compensate for Doppler-dependent waveform perturbations within the individual pulses. Pulse compression is accomplished with zero-Doppler filters.

Pulse compression schemes for NLFM waveforms tend to be direct matched filters or correlators of the entire full-bandwidth NLFM waveform. This was presumed by Urkowitz and Bucci.[12] Butler[13] discusses using Surface Acoustic Wave (SAW) devices for compressing NLFM waveforms.

2 Overview & Summary

LFM chirp waveforms have been successfully employed in a number of high-performance radar systems, but suffer a SNR disadvantage compared to NLFM chirp waveforms which can be designed to suppress processing sidelobes without any additional filtering. However, NLFM waveforms are generally more difficult to process and have been reported to suffer in their ability to maintain their desired impulse response shape in the presence of significant intra-pulse Doppler shifts, that is, their Doppler tolerance.

Both LFM and NLFM waveforms can be treated as generalized FM chirp waveforms, for which range-Doppler processing can be devised that compensates for intra-pulse Doppler shifts. Such algorithms can even be adjusted to compensate for migration, equivalent to the Polar Format Algorithm for Synthetic Aperture Radar.

Consequently, NLFM waveforms are shown to be viable for high performance range-Doppler radar applications, readily offering their advantages over their LFM counterparts.

Section 3 details a number of basic principles of pulse-Doppler radar waveforms. Section 4 discusses a number of aspects of basic range-Doppler processing in the context of Moving Target Indicator (MTI) radar processing. Section 5 discusses SAR processing.

“There's a way to do it better - find it.”

Thomas A. Edison

3 Basic Principles

3.1 The Received Echo from a Single Pulse

Consider a single pulse from a pulsed radar system with transmit waveform described by

$$x_T(t) = A_T(t)\exp\{j(\zeta_T(t) + 2\pi f_0 t)\} \tag{1}$$

where

t = time variable,
$A_T(t)$ = transmitted pulse envelope function,
$\zeta_T(t)$ = baseband phase modulation function, and
f_0 = nominal center frequency of the signal. (2)

Since modern radar systems' power amplifiers typically operate in compression, applying a precision amplitude taper to a pulse is generally difficult, and in some cases not even possible. Consequently we limit our attention to finite rectangular pulses with shape

$$A_T(t) = a_T \operatorname{rect}\left(\frac{t}{T}\right) \tag{3}$$

where

a_T = amplitude of the pulse,
T = pulse width, and

$$\operatorname{rect}(z) = \begin{cases} 1 & |z| \le 1/2 \\ 0 & else \end{cases}. \tag{4}$$

We will also assume that the energy spectrum of $x_T(t)$ is centered at f_0 and effectively band-limited to a fraction of its center frequency.

It will be useful later to define the baseband modulation signal

$$x_0(t) = A_T(t)\exp\{j\zeta_T(t)\} \tag{5}$$

such that it modulates the carrier in the fashion

$$x_T(t) = x_0(t)\exp\{j2\pi f_0 t\}. \tag{6}$$

We shall presume that $\zeta_T(t)$ is even. This is quite common for NLFM signals. Consequently the spectrum of $x_0(t)$ will also exhibit even symmetry, and $x_T(t)$ will be even about its center frequency f_0. If we assume the transmitted signal is reflected by a distortionless isotropic point scatterer, then the echo signal is described by

$$x_R(t) = \frac{a_R}{a_T} x_T(t - t_s) \tag{7}$$

where

a_R = amplitude of the received pulse, and
t_s = echo delay time. (8)

The round-trip echo delay time is related to the range of the scatterer by the velocity of propagation by

$$t_s = \frac{2}{c} r_s \tag{9}$$

where

c = speed of propagation, and
r_s = range between radar and target. (10)

In general, this range is time-varying. We shall presume that it is adequately modeled as linear with time during the pulse. Consequently

$$r_s \to r_s + v_s \left(t - \frac{2}{c} r_s \right) \tag{11}$$

where

$$v_s = \frac{d}{dt} r_s . \tag{12}$$

Of course the echo time delay then also becomes time varying, that is

$$t_s \to t_s + \dot{t}_s (t - t_s) \tag{13}$$

where

$$\dot{t}_s = \frac{d}{dt} t_s = \frac{2}{c} v_s . \tag{14}$$

Note that a closing velocity is negative due to decreasing range with time. Incorporating the effects of velocity allows

$$x_R(t) = \frac{a_R}{a_T} x_T\left(t - t_s - \dot{t}_s(t - t_s)\right) = \frac{a_R}{a_T} x_T\left((1 - \dot{t}_s)(t - t_s)\right). \tag{15}$$

There are two important effects to be observed in the target echo signal. The first is that the pulse is delayed by t_s which corresponds to the nominal target range. This value is presumed constant during a single pulse echo.

The second manifestation is the scaling of time within a pulse due to the rate of change in echo delay $\dot{t}_s$, which in turn is due to the relative velocity between radar and target during the single pulse interrogation. This is also discussed by Rihaczek. The scaling property of the Fourier Transform indicates that a time scaling is equivalent to a frequency scaling. Frequency scaling is of course a frequency-dependent frequency shift. For narrow-band signals this is often adequately modeled as a uniform frequency shift, that is, a Doppler shift. In fact, it would be generally more accurate to describe this as a Doppler scaling.

We define the Fourier Transform pair

$$x_0(t) \leftrightarrow X_0(f). \tag{16}$$

Consequently, we can identify the transmit waveform Fourier Transform pair

$$x_T(t) \leftrightarrow X_T(f) = X_0(f - f_0). \tag{17}$$

The received signal's Fourier Transform pair then becomes

$$x_R(t) \leftrightarrow X_R(f) = \frac{a_R/a_T}{(1 - \dot{t}_s)} X_0\left(\frac{f}{(1 - \dot{t}_s)} - f_0\right) \exp\{-j2\pi t_s f\}. \tag{18}$$

A good approximation to this is

$$x_R(t) \leftrightarrow X_R(f) = \frac{a_R}{a_T} X_0\left(f(1 + \dot{t}_s) - f_0\right) \exp\{-j2\pi t_s f\}. \tag{19}$$

3.2 Radar Ambiguity Function

We ask the question "How well does the received signal match a simply delayed transmitted signal?"

The phase of the received signal is given by

$$\Phi_R(t) = \zeta_T\left((1 - \dot{t}_s)(t - t_s)\right) + 2\pi f_0 (1 - \dot{t}_s)(t - t_s). \tag{20}$$

The instantaneous frequency of the received signal is then given by

$$\omega_R(t) = \frac{d}{dt}\Phi_R(t) = \left[\frac{d}{dt}\zeta_T(t) + 2\pi f_0\right](1 - \dot{t}_s). \tag{21}$$

Under narrowband conditions, this can be approximated as

$$\omega_R(t) = \left[\frac{d}{dt}\zeta_T(t) + 2\pi f_0\right] - 2\pi f_0 \dot{t}_s \tag{22}$$

We identify as the nominal Doppler shift

$$f_d = -f_0 \dot{t}_s \tag{23}$$

where positive Doppler is for diminishing range. This allows us to approximate the received signal as

$$x_R(t) = a_R \operatorname{rect}\left(\frac{t - t_s}{T}\right)\exp\{j(\zeta_T(t - t_s) + 2\pi f_0(t - t_s) + 2\pi f_d(t - t_s))\} \tag{24}$$

We identify the reference signal as the delayed transmitted signal, namely

$$x_\Delta(t) = a_T \operatorname{rect}\left(\frac{t - t_\Delta}{T}\right)\exp\{j(\zeta_T(t - t_\Delta) + 2\pi f_0(t - t_\Delta))\} \tag{25}$$

where

$$t_\Delta = \text{reference delay.} \tag{26}$$

The similarity function is the following inner product

$$\chi(t_s, t_\Delta, f_d) = \int_{-\infty}^{\infty} x_\Delta^*(t) x_R(t) dt\,. \tag{27}$$

where the asterisk superscript denotes complex conjugate. Since we are interested in similarity of shape, we can presume that envelope amplitudes are similar, that is, we shall presume that $a_R = a_T$. Consequently,

$$\chi(t_s, t_\Delta, f_d) = \int_{-\infty}^{\infty} x_T^*(t - t_\Delta) x_T(t - t_s)\exp\{j2\pi f_d(t - t_s)\} dt\,. \tag{28}$$

which can be written with a substitution of variables as

$$\chi(\tau, f_d) = \int_{-\infty}^{\infty} x_T^*(t+\tau) x_T(t) \exp\{j2\pi f_d t\} dt \tag{29}$$

where

$$\tau = t_s - t_\Delta \,. \tag{30}$$

The magnitude squared of this function $|\chi(\tau, f_d)|^2$ is in fact the common definition of the radar ambiguity function.[14] It is a measure of the similarity of the transmitted signal with both a time shifted and Doppler shifted echo signal. Note that the inherent assumption of the Doppler shift is that the transmitted signal is effectively narrow band.

A more generalized expression would be

$$\chi(t_s, t_\Delta, \dot{t}_s) = \int_{-\infty}^{\infty} x_T^*(t - t_\Delta) x_T((1-\dot{t}_s)(t - t_s)) dt \,. \tag{31}$$

or with a couple changes of variables

$$\chi(\tau, \dot{\tau}) = \int_{-\infty}^{\infty} x_T^*(t+\tau) x_T((1-\dot{\tau})t) dt \,. \tag{32}$$

Some comments are in order.

- The ambiguity function is a quasi-popular tool for evaluating waveforms for radar applications.
- As previously stated, the common form of the ambiguity function does make an inherent assumption of essentially narrow-band waveforms.
- In general, as Doppler shift or scaling increases, the ambiguity function's output value diminishes from its peak value. This is because the ambiguity function matches against the case of a reference signal with no Doppler.
- The ambiguity function with no Doppler shift is essentially an autocorrelation function, albeit with a sign change in τ. This is immaterial for an even autocorrelation function.
- Wideband waveforms would be more accurately evaluated using the more generalized expression.

We also note that as a measure of matched filter output, the general form also ignores the fact that if $\dot{\tau}$ were known, then the matched filter could be adjusted accordingly. Doing so should restore performance lost due to Doppler intolerance.

3.3 Pulse Compression

We now explore some details of compressing a single pulse with a matched filter.

Pulse compression is accomplished by making a similarity measure of an input signal with the expected pulse response. We identify the similarity measure for this purpose as the cross correlation operation of an input $x(t)$ with a reference signal $g(t)$ as

$$y(t) = \text{xcorr}(g(t), x(t)) = \int_{-\infty}^{\infty} g^*(-u)x(t-u)du = \int_{-\infty}^{\infty} g^*(u)x(u+t)du \tag{33}$$

and recall that this is related to convolution as

$$y(t) = \text{xcorr}(g(t), x(t)) = g^*(-t) * x(t). \tag{34}$$

In terms of their Fourier Transforms, cross correlation implies

$$Y(f) = G^*(f)X(f) \tag{35}$$

where we identify the Fourier pairs

$$\begin{aligned} &x(t) \leftrightarrow X(f), \\ &g(t) \leftrightarrow G(f), \\ &y(t) \leftrightarrow Y(f). \end{aligned} \tag{36}$$

A filter $h(t)$ that provides the same result as correlation with $g(t)$ has the form

$$h(t) = g^*(-t) \tag{37}$$

or, in the frequency domain

$$H(f) = G^*(f) \tag{38}$$

where

$$h(t) \leftrightarrow H(f). \tag{39}$$

Consequently, the filtering operation is given in the time domain as

$$y(t) = h(t) * x(t) \tag{40}$$

and in the frequency domain as

$$Y(f) = H(f)X(f). \tag{41}$$

Since $g(t)$ represents the desired response, then $h(t)$ is the matched filter for the desired signal. Since they provide equivalent results, we will henceforth use the terms matched filter interchangeably with correlation.

Recall the output of a matched filter, when input with the signal to which it is matched, is the autocorrelation of the signal. Recall also that the autocorrelation function is related to the energy spectrum of the desired signal via a Fourier Transform. We now define

$$S(f - f_0) = \text{radar signal energy spectrum of the desired signal} \tag{42}$$

where $S(f)$ is real, band-limited, and even. Consequently, the autocorrelation function can be written as

$$R(\tau) = W(\tau)\exp(j2\pi\, f_0\tau) \tag{43}$$

where $W(\tau)$ is also real-valued and even. $W(\tau)$ defines the shape of the matched filter output. Furthermore, for signals of interest to us, $W(\tau)$ exhibits a single main lobe. The phase within the mainlobe, however, depends on delay offset τ and is proportional to signal center frequency f_0.

Of significance to Doppler processing, subtle changes in range between radar and target causes a subtle change in the echo delay time of the pulse, which causes a noticeable phase rotation in the output of a filter matched to a particular delay. This is essential to range-Doppler processing, including SAR processing.

3.4 Multiple Pulses

If we consider multiple pulses from the radar system, then the transmitted signal for a member of a set of pulses is described by

$$x_T(t,n) = A_T(t - t_n)\exp\{j(\zeta_T(t - t_n, n) + 2\pi f_n(t - t_n))\} \tag{44}$$

where

n = pulse index number, $-N/2 \le n < N/2$,
t_n = reference time for the nth pulse, and
f_n = the center frequency of the nth pulse. (45)

The received signal is modified to

$$x_R(t,n) = \frac{a_R}{a_T} x_T\left((1 - \dot{t}_{s,n})(t - t_n - t_{s,n}), n\right) \tag{46}$$

where the index has been added as a subscript to variables that may change on a pulse-to-pulse basis.

There are two important manifestations of radar motion to be observed. The first is a pulse-to-pulse delay change $t_{s,n}$ due to range change. This is the manifestation that leads to pulse-to-pulse echo phase changes that are taken as the Doppler information for conventional SAR processing, providing azimuth resolution enhancement.

The second is the true Doppler scaling within a single pulse, sometimes called "intra-pulse Doppler" to differentiate it from the "inter-pulse Doppler" conventionally measured by SAR. This intra-pulse Doppler is typically ignored by most SAR systems, although it can become significant and needs to be accounted for in high-performance SAR systems. It is often cited as more problematic for waveforms other than LFM than for LFM waveforms, and for applications other than SAR, such as weather radar.

Ignoring the intra-pulse Doppler is the basis for assuming the "stop and go" model for range-Doppler processing, which acknowledges that the radar position with respect to the target changes from pulse to pulse, but during any single pulse all relative motion stops and range is presumed constant. While this clearly isn't true, it is often a 'good enough' presumption for radar system design, operation, and processing - just not always.

3.5 Geometry Details

Consider the geometry as defined in Figure 1.

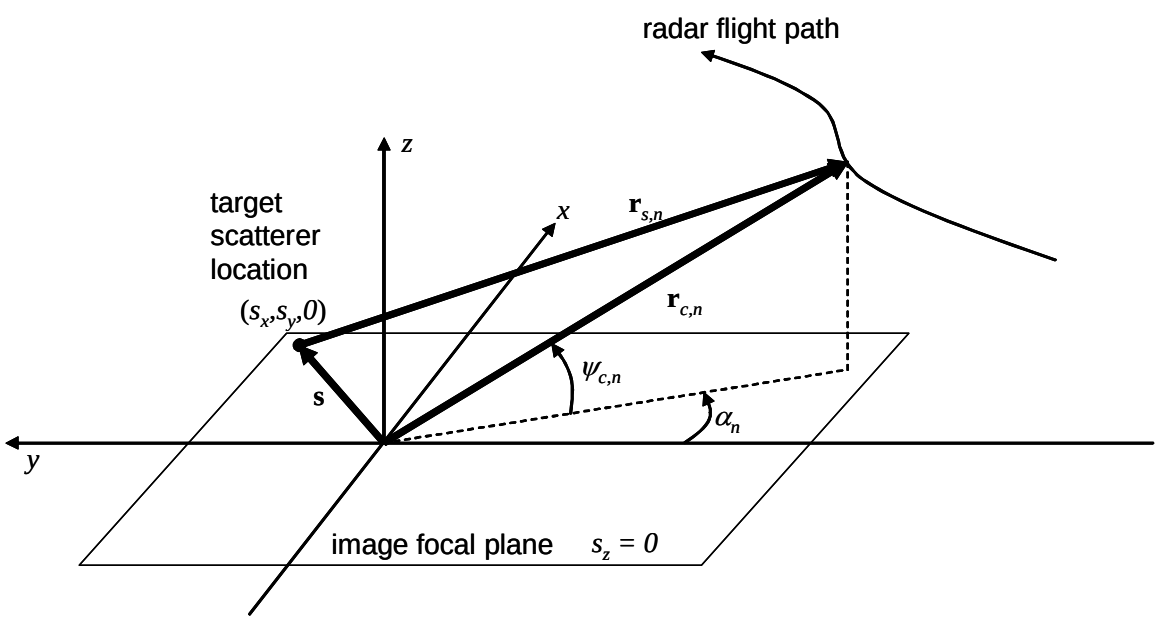

Figure 1. Geometry definitions.

The geometry will not be static, due to motion of the radar and/or target. We shall consider the dynamic geometry in two parts. First we shall consider variations from pulse to pulse, assuming the stop-and-go model. Second we will consider the velocity during the time of the pulse itself.

For a single pulse with index *n*, the radar is located in this frame at vector location $\mathbf{r}_{c,n}$, and the target scattering point is located at vector location $\mathbf{s}_n$ with coordinates $(s_{x,n}, s_{y,n}, 0)$. In general we will allow the target location to change from pulse to pulse with a constant velocity. Consequently,

$$\mathbf{s}_n = \mathbf{s}_0 + \mathbf{v}_t\left(t_n + t_{s,n} - t_{ref}\right) \tag{47}$$

where

$$t_{ref} \text{ = a reference time for the entire synthetic aperture, and} \tag{48}$$
$$\mathbf{v}_t \text{ = relative velocity vector of target point with respect to target scene center,}$$

and we identify the components of $\mathbf{v}_t$ as (v_{sx}, v_{sy}, v_{sz}). Then we identify the vector from target to radar as

$$\mathbf{r}_{s,n} = \mathbf{r}_{c,n} - \left(\mathbf{s}_0 + \mathbf{v}_t\left(t_n + t_{s,n} - t_{ref}\right)\right) \tag{49}$$

We note that the range to the target point is

$$r_{s,n} = \left|\mathbf{r}_{s,n}\right|. \tag{50}$$

Similarly, we define the reference range to the scene center as

$$r_{c,n} = \left|\mathbf{r}_{c,n}\right|. \tag{51}$$

Variations in $\mathbf{r}_{c,n}$ as a function of index *n* defines the synthetic aperture. We do not require the radar motion to exhibit constant velocity, and therefore keep its notation general. We shall use the common expansion for a target moving with constant velocity and allow the approximation

$$r_{s,n} \approx r_{c,n} + \begin{pmatrix} \cos\psi_{c,n}\cos\alpha_n\left(s_y + v_{sy}\left(t_n + t_{s,n} - t_{ref}\right)\right) \\ -\cos\psi_{c,n}\sin\alpha_n\left(s_x + v_{sx}\left(t_n + t_{s,n} - t_{ref}\right)\right) \end{pmatrix}. \tag{52}$$

During the pulse, the relevant motion for Doppler is the line-of-sight velocity from target point to radar. We calculate this as

$$v_{s,n} = \frac{\mathbf{r}_{s,n}}{\left|\mathbf{r}_{s,n}\right|} \bullet \frac{d}{dt}\mathbf{r}_{s,n} = \frac{\mathbf{r}_{s,n}}{\left|\mathbf{r}_{s,n}\right|} \bullet \mathbf{v}_{s,n} \tag{53}$$

where

$\mathbf{v}_{s,n}$ = relative velocity vector of radar with respect to target for pulse *n*. (54)

We will use the convention that a positive scalar velocity indicates an increasing distance between target and radar. For the general case of a moving target point and a moving radar

$$\mathbf{v}_{s,n} = \mathbf{v}_{c,n} - \mathbf{v}_t \tag{55}$$

where

$\mathbf{v}_{c,n}$ = relative velocity vector of radar with respect to target scene center, (56)

and we identify the components of $\mathbf{v}_{c,n}$ as $\left(v_{cx,n}, v_{cy,n}, v_{cz,n}\right)$. The line-of-sight velocity of the radar with respect to the target scene center is

$$v_{c,n} = \frac{\mathbf{r}_{c,n}}{\left|\mathbf{r}_{c,n}\right|} \bullet \mathbf{v}_{c,n} = \cos\psi_{c,n} \sin\alpha_n v_{cx,n} - \cos\psi_{c,n} \cos\alpha_n v_{cy,n} \,. \tag{57}$$

The component of the target point velocity aligned with the direction to the target scene center is

$$v_{t,n} = \frac{\mathbf{r}_{c,n}}{\left|\mathbf{r}_{c,n}\right|} \bullet \mathbf{v}_t = \cos\psi_{c,n} \sin\alpha_n v_{sx} - \cos\psi_{c,n} \cos\alpha_n v_{sy} \,. \tag{58}$$

Note that although the target velocity vector is constant, its projection in the direction of the radar will in fact change with changing position of the radar. Consequently we can approximate the velocity in the direction of the target point scatterer as approximately

$$v_{s,n} \approx v_{c,n} - v_{t,n} - \frac{v_{cx,n} s_x + v_{cy,n} s_y}{r_{c,n}} + \frac{v_{sx,n} s_x + v_{sy,n} s_y}{r_{c,n}} \,. \tag{59}$$

<u>Slant Range Coordinates</u>

There will be occasions when it is more useful to use slant-range coordinates for position s_r and velocity v_{sr}, where

$$r_{s,n} - r_{c,n} \approx s_r + v_{sr}\left(t_n + t_{s,n} - t_{ref}\right). \tag{60}$$

3.6 Intra-Pulse Doppler – When is it Significant?

Since intra-pulse Doppler is seemingly an issue with at least some waveforms, a prudent question might be "Under what circumstances is intra-pulse Doppler significant?"

Recall that we presume the energy spectrum for a pulse with index *n* to be band-limited and even about its center frequency f_n. We shall presume the signal has bandwidth B_n.

A relative velocity with respect to the target point will scale frequencies such that the echo exhibits a new center frequency $(1-\dot{t}_{s,n})f_n$ and bandwidth $(1-\dot{t}_{s,n})B_n$. Over some measurement time, say the transmitted pulse width *T*, then the echo will exhibit phase changes that depart from the transmitted phase linearly with time. Since coherent pulse compression relies on precise phase relationships being held, the departure from the expected phase with time will cause a degradation in the matched filter output. Using the center frequency f_n as a reasonably representative frequency value, we then desire to cap the phase error via the relationship

$$\left|2\pi f_n \dot{t}_{s,n} T\right| < \phi \tag{61}$$

where

$$\phi = \text{allowable phase error.} \tag{62}$$

Recalling that $f_n \dot{t}_{s,n}$ is the Doppler term, this relationship is identical to that given by Urkowitz and Bucci, among others. A typical number for ϕ for low-frequency non-sinusoidal errors (e.g. quadratic, etc.) might be on the order of $\pi/5$, although this number is somewhat squishy. To simplify notation, we will henceforth presume $\dot{t}_{s,n}$ to be positive, and recall its expansion $\dot{t}_{s,n} = 2v_{s,n}/c$. Some interesting variants of the inequality can then be developed. For example, some rearranging allows

$$v_{s,n}T < \frac{1}{2}\left(\frac{\phi}{2\pi}\right)\lambda_n . \tag{63}$$

where

$$\lambda_n = c/f_n = \text{the nominal wavelength of the radar.} \tag{64}$$

This suggests that the range-change during the pulse $(v_{s,n}T)$ needs to be substantially less than the nominal wavelength of the radar. Given the typical limit $\phi = \pi/5$, this suggests that

$$v_{s,n}T < \lambda_n/20 . \tag{65}$$

For example, a 2 cm wavelength would allow a 1 mm range change during the pulse. For a 10 μs pulse, this allows up to 100 m/s for a closing velocity. Higher velocities would require shorter pulses to be used, unless other mitigation schemes were employed.

For large time-bandwidth signals typical of high-performance radars, where $B_n T >> 1$, the inequality can be rearranged to

$$\dot{t}_{s,n} f_n << \left(\frac{\phi}{2\pi} \right) B_n \,. \tag{66}$$

This yields the necessary, but not sufficient, condition that the Doppler shift/scaling needs to be much less than the bandwidth of the signal.

Putting some perspective on $\dot{t}_{s,n}$, we calculate that for $v_{s,n} = 150$ m/s then $\dot{t}_{s,n} = 10^{-6}$. For a 2 cm wavelength, this amounts to a 15 kHz shift.

For further perspective, a ground vehicle moving at 50 mph is traveling at 22.4 m/s. An aircraft flying at 200 kts is traveling at 102.9 m/s. A hurricane by definition has wind speeds greater than 33 m/s. A category 5 hurricane has speeds greater than 69 m/s.

This suggests that radars designed to detect and measure moving targets, whether vehicles, aircraft, or weather, using pulses with lengths in the tens of microseconds will likely have to acknowledge and deal with intra-pulse Doppler to achieve maximum performance.

Note that for this constraint we have used no specific assumptions of any particular waveform other than it having finite bandwidth significantly less than its center frequency.

<u>Synthetic Aperture Radar</u>

With SAR the target is presumed stationary, however relative motion still exists due to the motion of the radar. The radar's antenna will illuminate a patch of the ground, which will exhibit a range of relative velocities with respect to the radar. Hence the range of Doppler frequencies will exhibit some spread or bandwidth related to the radar antenna's beamwidth, more specifically its beam footprint.

Since SAR requires some transverse motion with respect to the target scene, the relative motion between radar and target points will exhibit less velocity than the aircraft's forward motion would otherwise suggest.

Two aspects of the relative velocity become important for intra-pulse Doppler;

1) the relative velocity of a target point in the center of the target scene, and

2) the spread of velocities within the scene, which is limited by the antenna beam.

Recall that the relative velocity of an aircraft with respect to a stationary target point at the scene center is given by

$$v_{c,n} = \frac{\mathbf{r}_{c,n}}{\left|\mathbf{r}_{c,n}\right|} \bullet \mathbf{v}_{c,n} \,. \tag{67}$$

For level, straight-line flight, and measured at the nominal center of the synthetic aperture, this can be written as

$$v_{c,0} = \cos\psi_{c,0} \cos\Theta_s v_{aircraft} \tag{68}$$

where

Θ_s = the nominal squint angle, and

$v_{aircraft}$ = the forward speed of the aircraft. (69)

The nominal squint angle is measured in the target ground plane as the difference between the radar travel direction, and the bearing to the target scene center. The case $\Theta_s = 90$ degrees corresponds to a broadside direction.

For perspective, a radar flying at 300 kts and imaging with a nominal 2 cm wavelength at a 45 degree squint, and at a 30 degree grazing angle, will exhibit a relative velocity with respect to the target scene center of 94.5 m/s. From above we calculate that intra-pulse Doppler will need to be mitigated if a pulse longer than 10.6 μs is used, and this is just to properly focus the scene center.

The range of velocities within the field of view of the radar is constrained by the antenna beam footprint to approximately

$$\left(\cos\left(\varphi + \frac{\theta_{az}}{2}\right) v_{aircraft}\right) \le v_{s,0} \le \left(\cos\left(\varphi - \frac{\theta_{az}}{2}\right) v_{aircraft}\right) \tag{70}$$

where

$\cos(\varphi) = \cos\psi_{c,0} \cos\Theta_s$, and

θ_{az} = the azimuth beamwidth of the antenna. (71)

Note that φ is the squint angle in the slant plane. While some dependence exists on the elevation beamwidth, for the typical narrow-beam antennas used for SAR the principal dependence is on the azimuth beamwidth.

For a narrow-beam antenna with a not-too-severe squint, the velocity difference between beam edge and beam center is approximately

$$\Delta v_{s,0} \approx v_{aircraft} \sin\frac{\theta_{az}}{2} \sin\varphi = v_{aircraft} \sin\frac{\theta_{az}}{2} \sqrt{1-\cos^2\psi_{c,0}\cos^2\Theta_s} \ . \tag{72}$$

The implication is that even if intra-pulse Doppler could be mitigated for the scene center, if no additional corrections are made then targets at the beam edge would still exhibit residual intra-pulse Doppler due to their relative velocity with respect to the scene center.

For perspective, we return to the previous example of a radar with nominal 2 cm wavelength flying at 300 kts and imaging at a 45 degree squint, and at a 30 degree grazing angle, but now compensated for a relative velocity with respect to the target scene center of 94.5 m/s. If we further assume a 5 degree azimuth beamwidth for the antenna, then the relative velocity at the beam edge would be 5.32 m/s. This now allows a pulse width of up to 188 μs before additional intra-pulse Doppler mitigation is required.

As another example, consider a radar with nominal 13 cm wavelength placed in Low-Lunar-Orbit (LLO), where the forward velocity is 1630 m/s, and imaging broadside at a 45 degree grazing angle with an azimuth beamwidth of 4.6 degrees. The relative velocity at the beam edge would be 65.4 m/s. This now allows a pulse width of 99.4 μs before additional intra-pulse Doppler mitigation is required.

As a final example, consider a radar with nominal 2 cm wavelength placed in Low-Earth-Orbit (LEO), where the forward velocity is 7300 m/s, and imaging broadside at a 45 degree grazing angle with an azimuth beamwidth of 0.5 degrees. The relative velocity at the beam edge would be 31.9 m/s. This now allows a pulse width of 31.4 μs before additional intra-pulse Doppler mitigation is required.

Recalling that our threshold was somewhat squishy to begin with, these examples suggest that for SAR, once intra-pulse Doppler is compensated to the scene center, variations in intra-pulse Doppler across the scene are likely to not be problematic for many systems. Indeed, Curlander and McDonough[15] conclude for a side-looking SAR using an LFM chirp "any defocusing due to distortion of the received pulse [from intra-pulse Doppler scaling] is negligible."

The prudent designer would nevertheless double-check this to be sure.

4 Simple Range and Doppler Measurements

To illustrate some basic principles of range-Doppler radars, we begin with some very basic examples. We shall continue to presume that the energy spectrum is real, band-limited, and even about its center at f_n. In fact, for this section we shall presume a constant transmit waveform from pulse to pulse with center frequency f_0, that is

$$f_n = f_0 . \tag{73}$$

We shall furthermore assume that the radar is stationary, and the target point is moving with a constant non-zero line-of-sight velocity. This is the case for a simple Moving Target Indicator (MTI) radar.

The received signal from a single distortionless isotropic point scatterer is still adequately modeled by

$$x_R(t) = \frac{a_R}{a_T} x_T\left(\left(1-\dot{t}_s\right)\left(t-t_s\right)\right). \tag{74}$$

We shall furthermore assume the slant-range expansion

$$r_{s,n} \approx r_{c,n} + \left(s_r + v_{sr}\left(t_n + t_{s,n} - t_{ref}\right)\right). \tag{75}$$

This can be manipulated to

$$r_{s,n} \approx r_{c,n} + \left(s_r + v_{sr}\left(t_{s,n} - t_{c,n}\right) + v_{sr}\left(t_n + t_{c,n} - t_{ref}\right)\right). \tag{76}$$

We choose a reference time, and pulse times at

$$t_n + t_{c,n} - t_{ref} = T_p n \tag{77}$$

where

$$T_p = \text{the constant pulse period.} \tag{78}$$

We note that T_p is the inverse of the Pulse Repetition Frequency (PRF). Nevertheless, this allows

$$r_{s,n} \approx r_{c,n} + \left(s_r + v_{sr}\left(t_{s,n} - t_{c,n}\right) + v_{sr} T_p n\right). \tag{79}$$

Typically, $v_{sr}\left(t_{s,n} - t_{c,n}\right)$ is much smaller than the range resolution of the radar. Consequently it can typically be ignored, allowing the approximation

$$r_{s,n} \approx r_{c,n} + \left(s_r + v_{sr} T_p n\right). \tag{80}$$

We furthermore identify the intra-pulse Doppler as dependent on the relevant velocity components as

$$v_{s,n} \approx v_{sr}\,. \tag{81}$$

4.1 Time-Domain Processing – Negligible Intra-Pulse Doppler

In this section we employ direct time-domain correlation to the received echo signal to ascertain range.

Assuming that intra-pulse Doppler is negligible, the received signal can be simplified to

$$x_R(t,n) = \frac{a_R}{a_T} x_T\left(t - t_n - t_{s,n}, n\right). \tag{82}$$

We shall first correlate this against a delayed reference signal of the form

$$x_m(t,n) = \frac{1}{a_T} x_T\left(\left(t - t_n - t_{c,n}\right), n\right). \tag{83}$$

The output is given by

$$y(t,n) = \mathrm{xcorr}\left(x_m(t,n), x_R(t,n)\right) = \int_{-\infty}^{\infty} x_m^*(u,n) x_R(u+t,n)\,du \tag{84}$$

and results in

$$y(t,n) = a_R W_t\left(t - \left(t_{s,n} - t_{c,n}\right)\right) \exp\left\{ j2\pi f_0 \left(t - \left(t_{s,n} - t_{c,n}\right)\right)\right\} \tag{85}$$

where

$$W_t(t) = \text{the range impulse response envelope of the correlation output.} \tag{86}$$

$W_t(t)$ is real valued, and has a peak at $W_t(0)$. This occurs when

$$t = \left(t_{s,n} - t_{c,n}\right) \tag{87}$$

which occurs when

$$t = \frac{2}{c}\left(r_{s,n} - r_{c,n}\right) = \frac{2}{c}\left(s_r + v_{sr}T_p n\right). \tag{88}$$

In this formulation we digitize the signal at sample times

$$t = \left(\frac{2}{c}\delta_r\right)k \tag{89}$$

where

δ_r = the range sample spacing, and
k = the compressed range index, $-K/2 \le k < K/2$. (90)

The peak response occurs for

$$\delta_r k = \left(s_r + v_{sr}T_p n\right). \tag{91}$$

The range compressed signal is now modeled as

$$y(k,n) = a_R W_t\left(\frac{2}{c}\left(\delta_y k - \left(s_r + v_{sr}T_p n\right)\right)\right)\exp\left\{j2\pi f_0\left(\frac{2}{c}\right)\left(\delta_y k - \left(s_r + v_{sr}T_p n\right)\right)\right\}. \tag{92}$$

Clearly, the peak index k is proportional to s_r, which is desirable, but also depends on v_{sr}, which is not desirable. This dependence on v_{sr} is range migration that will compromise focusing especially at finer resolutions. At coarser resolutions its effects are not too severe, and therefore often tolerable without any additional mitigation. If not too severe, this migration dependence on v_{sr} can be ignored. This allows the range compressed signal to be modeled as

$$y(k,n) = a_R W_t\left(\frac{2}{c}\left(\delta_r k - s_r\right)\right)\exp\left\{j2\pi f_0\left(\frac{2}{c}\right)\left(\delta_r k - \left(s_r + v_{sr}T_p n\right)\right)\right\}. \tag{93}$$

and then rewritten as

$$y(k,n) = a_R W_t\left(\left(\frac{2}{c}\right)\left(\delta_r k - s_r\right)\right)\exp\left\{j\frac{4\pi f_0}{c}\left(-v_{sr}T_p n\right)\right\}\exp\left\{j\frac{4\pi f_0}{c}\left(\delta_r k - s_r\right)\right\}. \tag{94}$$

The second exponential (second phase term) is inconsequential to further processing and can be ignored, which we will do. This allows the simpler model

$$y(k,n) = a_R W_t\left(\frac{2}{c}\left(\delta_r k - s_r\right)\right)\exp\left\{j\frac{4\pi f_0}{c}\left(-v_{sr}T_p n\right)\right\}. \tag{95}$$

Note that index *n* occurs only in the phase term of this expression, and that this term is linear in index *n*. To extract the estimate for v_{sr} we employ an Inverse Discrete Fourier Transform (IDFT) across index *n*. This yields the complex range-Doppler map target response

$$z(k,u) = a_R W_t\left(\frac{2}{c}(\delta_r k - s_r)\right) W_d\left(-\frac{4\pi f_0}{c} v_{sr} T_p + \frac{2\pi}{U} u\right) \tag{96}$$

where

$W_d(x)$ = the velocity impulse response envelope of the transform output,
u = the compressed azimuth index, $-U/2 \le u < U/2$. (97)

In general, the azimuth transform output has a phase component that goes along with $W_d(x)$, but this will be inconsequential to the complex range-Doppler map. Hence, we have ignored it. We have also kept notation of the velocity Impulse Response (IPR) general to allow for the use of window functions for velocity sidelobe control. In the absence of any additional range sidelobe filtering, the range sidelobes will correspond to the autocorrelation function of the transmitted waveform. The complex range-Doppler map target response can then be rearranged to a form

$$z(k,u) = a_R W_t\left(\frac{2}{c}(\delta_r k - s_r)\right) W_d\left(\frac{4\pi f_0}{c} T_p(\delta_{vr} u - v_{sr})\right) \tag{98}$$

where

δ_{vr} = the velocity sampling spacing. (99)

With this model, a target reflector with location specified by s_r and velocity component v_{sr} will cause a unique peak response at a corresponding range-Doppler map location $\delta_r k$ and $\delta_{vr} u$.

The processing steps are illustrated in Figure 2. While processing in this manner is well understood, we have presented it here as a baseline to understand subsequent enhancements.

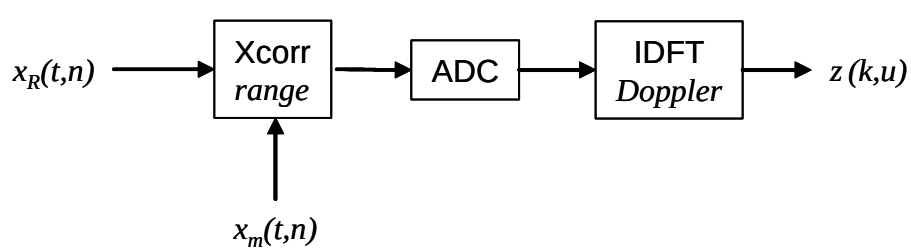

Figure 2. Simple range correlator followed by Doppler processing.

4.2 Frequency-Domain Processing – Negligible Intra-Pulse Doppler

In this section we employ frequency-domain filtering to implement the correlation of the received echo signal to ascertain range.

Assuming that intra-pulse Doppler is negligible, recall that the received signal can be simplified to

$$x_R(t,n) = \frac{a_R}{a_T} x_T\left(t - t_n - t_{s,n}, n\right) \tag{100}$$

with spectrum

$$X_R(f,n) = \frac{a_R}{a_T} X_0(f - f_0, n)\exp\left\{-j2\pi t_{s,n} f\right\}. \tag{101}$$

We select as the delayed reference signal

$$x_m(t,n) = \frac{1}{a_T} x_T\left(\left(t - t_n - t_{c,n}\right), n\right) \tag{102}$$

with spectrum

$$X_m(f,n) = \frac{1}{a_T} X_0(f - f_0, n)\exp\left\{-j2\pi t_{c,n} f\right\}. \tag{103}$$

The Fourier Transform of an analog correlator output can then be expressed as

$$Y(f,n) = X_m^*(f,n) X_R(f,n). \tag{104}$$

Recalling that the transmit waveform is constant, this can be expanded to

$$Y(f,n) = \begin{pmatrix} \frac{1}{a_T} X_0^*(f - f_0, 0)\exp\left\{j2\pi t_{c,n} f\right\} \\ \times \frac{a_R}{a_T} X_0(f - f_0, 0)\exp\left\{-j2\pi t_{s,n} f\right\} \end{pmatrix} \tag{105}$$

and then simplified to

$$Y(f,n) = a_R \left| \frac{X_0(f - f_0, 0)}{a_T} \right|^2 \exp\left\{-j2\pi\left(t_{s,n} - t_{c,n}\right) f\right\} \tag{106}$$

If the original signals had been sampled, and their Fourier Transforms calculated with a Discrete Fourier Transform (DFT), then we would have samples at discrete frequencies given by

$$f = f_0 + df_0\, i \tag{107}$$

where

f_0 = the center frequency of each pulse,
df_0 = the frequency sample increment for each pulse, and
i = the frequency index, $-I/2 \le i < I/2$. (108)

The digital correlator output signal spectrum would be

$$Y(i,n) = a_R \left| \frac{X_0(df_0\, i, 0)}{a_T} \right|^2 \exp\left\{ -j2\pi \left(t_{s,n} - t_{c,n} \right) \left(f_0 + df_0\, i \right) \right\}. \tag{109}$$

Observe that the magnitude-squared of the transmit-signal spectrum now constitutes a positive real-valued weighting function, behaving like a window or aperture weighting function, thereby influencing the shape of the ultimate range impulse response of the radar. Furthermore, the shape of this is exactly the ESD. We simplify this expression somewhat by identifying the equivalent weighting function explicitly as

$$w_r(i) = \left| \frac{X_0(df_0\, i, 0)}{a_T} \right|^2 . \tag{110}$$

Incorporating geometric definitions into this, and rearranging a bit yields

$$Y(i,n) = a_R w_r(i) \exp\left\{ -j \frac{4\pi f_0}{c} \left(1 + \frac{df_0}{f_0}\, i \right) \left(s_r + v_{sr} T_p n \right) \right\} \tag{111}$$

which can be rearranged to

$$Y(i,n) = a_R \left[\begin{array}{l} w_r(i) \exp\left\{ -j \dfrac{4\pi df_0}{c} s_r i \right\} \\ \times \exp\left\{ -j \dfrac{4\pi f_0}{c} v_{sr} T_p \left(1 + \dfrac{df_0}{f_0}\, i \right) n \right\} \\ \times \exp\left\{ -j \dfrac{4\pi f_0}{c} s_r \right\} \end{array} \right]. \tag{112}$$

This is now of a form that can be processed in a more conventional manner. We first make several observations.

- The second line in the square brackets has phase linear in index *n*, suggesting an IDFT to ascertain v_{sr} .

- The second line in the square brackets has phase also with a dependence on index *i*, which suggests undesirable migration if left unmitigated.

- The first term in the square brackets is linear in index *i*, suggesting an IDFT to ascertain s_r .

- In addition, the range dimension has a weighting function $w_r(i)$ effectively applied by virtue of the transmit waveform characteristics.

- Any shaping to mitigate sidelobes as a result of an IDFT across index *n* will require additional overt weighting applied.

- The third line in the square brackets is inconsequential to ascertaining range and velocity of the target point, and hence can be ignored.

The migration term can be mitigated by resampling the data such that

$$\left(1+\frac{df_0}{f_0}i'\right)n = n' . \tag{113}$$

This is essentially the approach taken by DiPietro, Perry, and Fante[16,17,18] to correct migration for moving targets. Whether resampled or ignored, the data model becomes

$$Y(i,n') = a_R w_r(i)\exp\left\{-j\frac{4\pi df_0}{c}s_r i\right\}\exp\left\{-j\frac{4\pi f_0}{c}v_{sr}T_p n'\right\}. \tag{114}$$

A 2D IDFT applied over indices i and n' will yield the range-Doppler map target response described by

$$z(k,u) = a_R W_r\left(-\frac{4\pi df_0}{c}s_r + \frac{2\pi}{K}k\right)W_d\left(-\frac{4\pi f_0}{c}v_{sr}T_p + \frac{2\pi}{U}u\right) \tag{115}$$

which can be rewritten in the form

$$z(k,u) = a_R W_r\left(\frac{4\pi df_0}{c}(\delta_r k - s_r)\right)W_d\left(\frac{4\pi f_0}{c}T_p(\delta_{vr}u - v_{sr})\right). \tag{116}$$

Comparing this to the results of the previous section, we identify

$$W_r(x) = W_t\left(\frac{x}{2\pi df_0}\right) \tag{117}$$

that is, they have the same shape but differ in the scaling of their input variable. This is due to $W_t(x)$ having been developed in terms of a time delay, and $W_r(x)$ having been developed in terms of phase. Nevertheless, they represent the same range IPR.

The processing steps are illustrated in Figure 3.

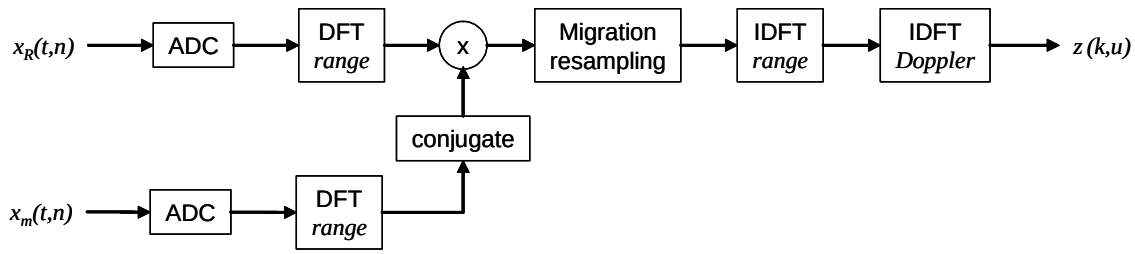

Figure 3. Frequency-domain processing with migration correction.

4.3 Compensating Intra-Pulse Doppler

In this section we continue to employ frequency-domain filtering to implement the correlation of the received echo signal to ascertain range, but now include the effects of intra-pulse Doppler. The model for the received signal that we begin with is

$$x_R(t,n) = \frac{a_R}{a_T} x_T\left(\left(1-\dot{t}_{s,n}\right)\left(t-t_n-t_{s,n}\right),n\right). \tag{118}$$

Since the transmitted signal is constant from pulse to pulse, we may presume $\dot{t}_{s,n} = \dot{t}_{s,0}$. The received signal spectrum is then

$$X_R(f,n) = \frac{a_R/a_T}{\left(1-\dot{t}_{s,0}\right)} X_0\left(\frac{f}{\left(1-\dot{t}_{s,0}\right)} - f_0, n\right)\exp\left\{-j2\pi t_{s,n} f\right\}. \tag{119}$$

We select as the delayed reference signal (without intra-pulse Doppler)

$$x_m(t,n) = \frac{1}{a_T} x_T\left(\left(t-t_n-t_{c,n}\right),0\right) \tag{120}$$

with spectrum

$$X_m(f,n) = \frac{1}{a_T} X_0(f-f_0,0)\exp\left\{-j2\pi t_{c,n} f\right\}. \tag{121}$$

The Fourier Transform of an analog correlator output can then be expressed as

$$Y(f,n) = X_m^*(f,n) X_R(f,n) \tag{122}$$

which can be expanded to

$$Y(f,n) = \begin{pmatrix} \frac{1}{a_T} X_0^*(f - f_0, 0) \exp\{j2\pi t_{c,n} f\} \\ \times \frac{a_R / a_T}{(1 - \dot{t}_{s,0})} X_0\left(\frac{f}{(1 - \dot{t}_{s,0})} - f_0, 0 \right) \exp\{-j2\pi t_{s,n} f\} \end{pmatrix} \tag{123}$$

and then simplified to

$$Y(f,n) = a_R \left[\frac{X_0^*(f - f_0, 0)}{a_T} \frac{X_0\left(\frac{f}{(1 - \dot{t}_{s,0})} - f_0, 0 \right)}{a_T (1 - \dot{t}_{s,0})} \right] \exp\{-j2\pi (t_{s,n} - t_{c,n}) f\}. \tag{124}$$

We expect $\dot{t}_{s,0}$ to generally be relatively small, such that we can approximate

$$Y(f,n) = a_R \left[\frac{X_0^*(f - f_0, 0)}{a_T} \frac{X_0(f - f_0 + \dot{t}_{s,0} f, 0)}{a_T} \right] \exp\{-j2\pi (t_{s,n} - t_{c,n}) f\}. \tag{125}$$

This can be rewritten as

$$Y(f,n) = \left(a_R \left| \frac{X_0(f - f_0, 0)}{a_T} \right|^2 \exp\{-j2\pi (t_{s,n} - t_{c,n}) f\} \right) H_{IPD}(f - f_0, \dot{t}_{s,0}) \tag{126}$$

where

$$H_{IPD}(f - f_0, \dot{t}_{s,0}) = \left(\frac{X_0(f - f_0 + \dot{t}_{s,0} f, 0)}{X_0(f - f_0, 0)} \right). \tag{127}$$

We clearly see that the effect of intra-pulse Doppler is to perturb the data in a manner equivalent to applying a filter to the data. To be sure, the filter is Doppler variant, that is, it depends on the location of the target in the range-Doppler map. This accounts for our overt inclusion of $\dot{t}_{s,0}$ as a parameter of H_{IPD}.

Some additional comments are in order.

- We can usually reasonably expect the Doppler shift at any frequency within the band to be small compared to the overall signal bandwidth. Consequently, the

envelopes of $X_0\left(f - f_0 + \dot{t}_{s,0} f, 0\right)$ and $X_0\left(f - f_0, 0\right)$ are expected to be very similar. This implies that $H_{IPD}\left(f - f_0, \dot{t}_{s,0}\right)$ is principally providing a phase function.

- The entity $H_{IPD}\left(f - f_0, \dot{t}_{s,0}\right)$ is in this model constant with index *n*.
- However, $H_{IPD}\left(f - f_0, \dot{t}_{s,0}\right)$ does depend on v_{sr}. Consequently, compensating for this perturbation requires first estimating v_{sr}.

Applying the sampling, resampling, and a number of the approximations in the previous section to this model yields

$$Y(i,n) = \begin{pmatrix} a_R w_r(i) \\ \times \exp\left\{ -j \frac{4\pi f_0}{c} \left(1 + \frac{df_0}{f_0} i \right) \left(s_r + v_{sr} T_p n \right) \right\} \end{pmatrix} H_{IPD}\left(df_0\, i, \dot{t}_{s,0}\right) \tag{128}$$

Ignoring constant phase terms, and mitigating migration, or simply ignoring the cross-coupling of indices *i* and *n* yields

$$Y(i,n') = \begin{pmatrix} a_R w_r(i) \exp\left\{ -j \frac{4\pi d f_0}{c} s_r i \right\} \\ \times \exp\left\{ -j \frac{4\pi f_0}{c} v_{sr} T_p n' \right\} \end{pmatrix} H_{IPD}\left(df_0\, i, \dot{t}_{s,0}\right) \tag{129}$$

An IDFT applied over index n' will yield the Doppler-compressed data described by

$$Y'(i,u) = \begin{pmatrix} a_R w_r(i) \\ \times \exp\left\{ -j \frac{4\pi d f_0}{c} s_r i \right\} \end{pmatrix} W_d\left(\frac{4\pi f_0}{c} T_p \left(\delta_{vr} u - v_{sr} \right) \right) H_{IPD}\left(df_0\, i, \dot{t}_{s,0}\right). \tag{130}$$

Since $Y'(i,u)$ has now resolved the velocity v_{sr}, we can now estimate $\dot{t}_{s,0}$ as well. This allows us to define $H_{IPD}\left(df_0\, i, \dot{t}_{s,0}\right)$ sufficiently to compensate for it. Consequently we calculate

$$Y''(i,u) = Y'(i,u) H_{IPD}^{-1}\left(df_0\, i, \dot{t}_{s,0}\right) \tag{131}$$

or

$$Y''(i,u) = \left(a_R w_r(i) \exp\left\{ -j \frac{4\pi d f_0}{c} s_r i \right\} \right) W_d\left(\frac{4\pi f_0}{c} T_p \left(\delta_{vr} u - v_{sr} \right) \right). \tag{132}$$

An IDFT across index i yields

$$z(k,u) = a_R W_r\left(\frac{4\pi d f_0}{c}\left(\delta_r k - s_r\right)\right) W_d\left(\frac{4\pi f_0}{c} T_p\left(\delta_{vr} u - v_{sr}\right)\right). \tag{133}$$

This result has mitigated the effects of intra-pulse Doppler in resolving the range-Doppler map target response.

The processing steps are illustrated in Figure 4.

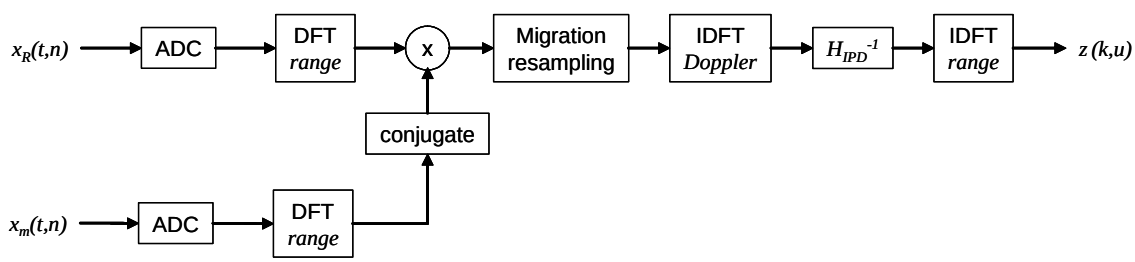

Figure 4. Frequency-domain processing with intra-pulse Doppler correction.

4.4 Compensating Intra-Pulse Doppler – Method 2

The model for the received signal that we again begin with is

$$x_R(t,n) = \frac{a_R}{a_T} x_T\left(\left(1-\dot{t}_{s,n}\right)\left(t - t_n - t_{s,n}\right), n\right). \tag{134}$$

Recalling that the transmitted signal is constant from pulse to pulse, this can be expanded to

$$x_R(t,n) = \frac{a_R}{a_T} x_0\left(\left(1-\dot{t}_{s,0}\right)\left(t - t_n - t_{s,n}\right), 0\right) \exp\left\{j2\pi f_0\left(1-\dot{t}_{s,0}\right)\left(t - t_n - t_{s,n}\right)\right\} \tag{135}$$

which can be further expanded to

$$x_R(t,n) = \frac{a_R}{a_T}\begin{pmatrix} x_0\left(\left(1-\dot{t}_{s,0}\right)\left(t - t_n - t_{c,n} - \left(t_{s,n} - t_{c,n}\right)\right), 0\right) \\ \times \exp\left\{-j2\pi f_0\left(1-\dot{t}_{s,0}\right)\left(t_{s,n} - t_{c,n}\right)\right\} \\ \times \exp\left\{-j2\pi f_0 \dot{t}_{s,0}\left(t - t_n - t_{c,n}\right)\right\} \\ \times \exp\left\{j2\pi f_0\left(t - t_n - t_{c,n}\right)\right\} \end{pmatrix}. \tag{136}$$

The fourth line in the parentheses is the carrier, and is easily compensated by mixing the signal to baseband. The third line is the Doppler offset of the nominal center frequency. The second line includes the phase variation that changes from pulse to pulse and is the conventional source for Doppler resolution. The first line is of course the modulation of the carrier that provides range resolution. Of all these, the principal effect of intra-pulse Doppler is on the shift of the center frequency in the third line, especially for relatively narrow-band modulation.

Consequently, we ignore the Doppler scaling in the first two lines, mix this signal to baseband, digitally sample it, and expand with geometric parameters to yield

$$x_V(i,n) \approx \frac{a_R}{a_T}\begin{pmatrix} x_0\left(\left(T_{s,0}i - \frac{2}{c}\left(s_r + v_{sr}T_p n\right)\right),0\right) \\ \times \exp\left\{-j\frac{4\pi f_0}{c}s_r\right\} \\ \times \exp\left\{-j2\pi f_0 \dot{t}_{s,0}T_{s,0}i\right\} \\ \times \exp\left\{-j\frac{4\pi f_0}{c}v_{sr}T_p n\right\} \end{pmatrix}. \tag{137}$$

An IDFT across the Doppler index n can resolve the velocity component v_{sr} and yield

$$y(i,u) \approx \frac{a_R}{a_T}\begin{pmatrix} x_0\left(\left(T_{s,0}i - \frac{2}{c}s_r\right),0\right) \\ \times \exp\left\{-j\frac{4\pi f_0}{c}s_r\right\} \\ \times \exp\left\{-j2\pi f_0 \dot{t}_{s,0}T_{s,0}i\right\} \end{pmatrix} W_d\left(\frac{4\pi f_0}{c}T_p\left(\delta_{vr}u - v_{sr}\right)\right). \tag{138}$$

This can in turn be used to estimate $\dot{t}_{s,0}$ which can be used to compensate the signal to yield

$$y'(i,u) = y(i,u)\exp\left\{j2\pi f_0 \dot{t}_{s,n}T_{s,0}i\right\} \tag{139}$$

or

$$y'(i,u) \approx \frac{a_R}{a_T}\begin{pmatrix} x_0\left(\left(T_{s,0}i - \frac{2}{c}s_r\right),0\right) \\ \times \exp\left\{-j\frac{4\pi f_0}{c}s_r\right\} \end{pmatrix} W_d\left(\frac{4\pi f_0}{c}T_p\left(\delta_{vr}u - v_{sr}\right)\right) \tag{140}$$

We have tacitly ignored migration due to the original dependence of $x_0\left(\left(T_{s,0}i-(2/c)(s_r+v_{sr}T_p n)\right),n\right)$ on index *n*. This is justified for relatively coarse resolutions in range and Doppler, and is adequate for compensating Doppler shift of the center frequency.

If migration is not problematic, then processing can be completed by simply correlating this response in the range dimension against $x_0\left(\left(T_{s,0}i\right),0\right)$. That is,

$$z(k,u)\approx \mathrm{xcorr}\left(\frac{x_0\left(T_{s,0}i,0\right)}{a_T},y'(i,u)\right). \tag{141}$$

This is illustrated in Figure 5. This approach which ignores the migration correction is essentially the technique described by Urkowitz and Bucci.

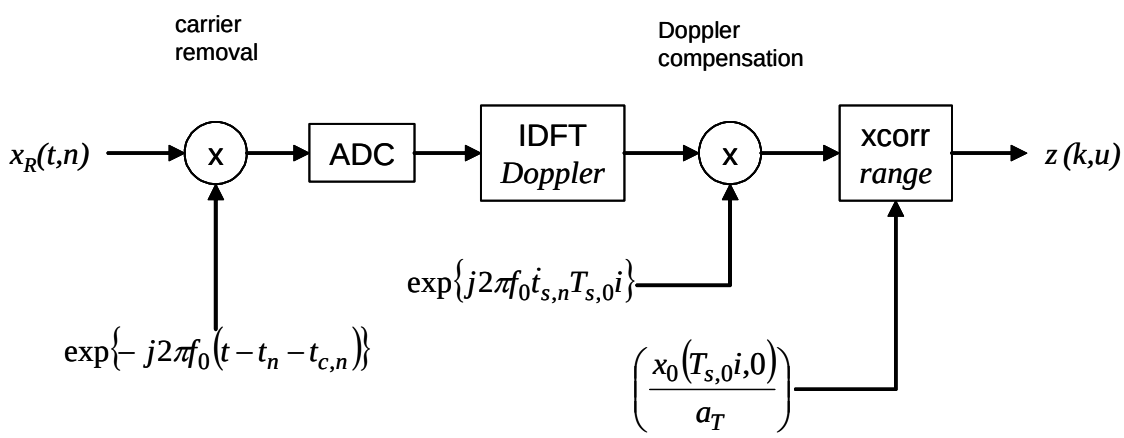

Figure 5. Technique described by Urkowitz and Bucci.

Mitigating migration can be achieved by somewhat more complex processing, by first undoing the Doppler IDFT, yielding

$$x_V'(i,n)\approx\frac{a_R}{a_T}x_0\left(\left(T_{s,0}i-\frac{2}{c}\left(s_r+v_{sr}T_p n\right)\right),0\right)\exp\left\{-j\frac{4\pi f_0}{c}\left(s_r+v_{sr}T_p n\right)\right\}. \tag{142}$$

We require entering the frequency domain of the modulation signal $x_0(t)$ by performing a DFT over index *i*, which yields

$$Y''(i',n)\approx\frac{a_R}{a_T}\left(\begin{array}{l}X_0(df_0 i',0)\exp\left\{-j\frac{4\pi}{c}\left(s_r+v_{sr}T_p n\right)df_0 i'\right\}\\ \times\exp\left\{-j\frac{4\pi f_0}{c}\left(s_r+v_{sr}T_p n\right)\right\}\end{array}\right) \tag{143}$$

which can be rearranged to

$$Y''(i',n) \approx \frac{a_R}{a_T}\begin{pmatrix} X_0(df_0 i',0)\exp\left\{-j\frac{4\pi}{c}s_r(f_0+df_0 i')\right\} \\ \times\exp\left\{-j\frac{4\pi f_0}{c}v_{sr}T_p\left(1+\frac{df_0}{f_0}i'\right)n\right\} \end{pmatrix}. \tag{144}$$

At this point we can multiply the data by the reference signal $X_0^*(df_0 i',0)/a_T$ to yield

$$Y'''(i',n) \approx a_R\begin{pmatrix} \left|\frac{X_0(df_0 i',0)}{a_T}\right|^2 \exp\left\{-j\frac{4\pi}{c}s_r(f_0+df_0 i')\right\} \\ \times\exp\left\{-j\frac{4\pi f_0}{c}v_{sr}T_p\left(1+\frac{df_0}{f_0}i'\right)n\right\} \end{pmatrix} \tag{145}$$

which we can simplify to

$$Y'''(i',n) \approx \begin{pmatrix} a_R w_r(i')\exp\left\{-j\frac{4\pi}{c}s_r(f_0+df_0 i')\right\} \\ \times\exp\left\{-j\frac{4\pi f_0}{c}v_{sr}T_p\left(1+\frac{df_0}{f_0}i'\right)n\right\} \end{pmatrix}. \tag{146}$$

Now that we are in the frequency domain, we can resample the data such that

$$\left(1+\frac{df_0}{f_0}i'\right)n = n' \tag{147}$$

which yields the migration corrected signal

$$Y'''(i',n') \approx \begin{pmatrix} a_R w_r(i')\exp\left\{-j\frac{4\pi}{c}s_r(f_0+df_0 i')\right\} \\ \times\exp\left\{-j\frac{4\pi f_0}{c}v_{sr}T_p n'\right\} \end{pmatrix}. \tag{148}$$

Ignoring the constant phase term furthermore yields

$$Y'''(i',n') \approx a_R w_r(i')\exp\left\{-j\frac{4\pi df_0}{c}s_r i'\right\}\exp\left\{-j\frac{4\pi f_0}{c}v_{sr}T_p n'\right\}. \tag{149}$$

As described in previous sections, a 2D IDFT applied over indices i' and n' will yield the range-Doppler map target response described by

$$z(k,u) = a_R W_r\left(\frac{4\pi d f_0}{c}\left(\delta_r k - s_r\right)\right) W_d\left(\frac{4\pi f_0}{c} T_p\left(\delta_{vr} u - v_{sr}\right)\right). \tag{150}$$

The processing steps are illustrated in Figure 6.

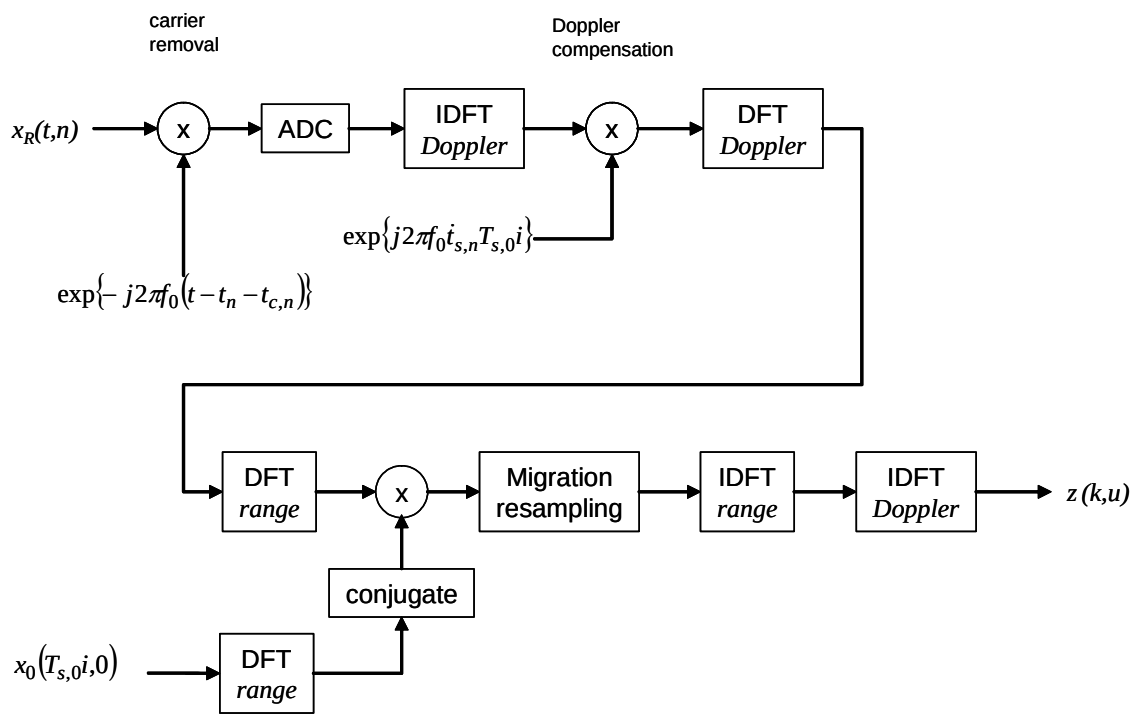

Figure 6. Technique described by Urkowitz and Bucci with added Migration compensation.

4.5 Compensating Intra-Pulse Doppler – Method 3

The model for the received signal that we again begin with is

$$x_R(t,n) = \frac{a_R}{a_T} x_T\left(\left(1 - \dot{t}_{s,n}\right)\left(t - t_n - t_{s,n}\right), n\right). \tag{151}$$

Recalling that the transmitted signal is constant from pulse to pulse, this can be expanded to

$$x_R(t,n) = \frac{a_R}{a_T} x_0\left(\left(1 - \dot{t}_{s,0}\right)\left(t - t_n - t_{s,n}\right), 0\right) \exp\left\{j2\pi f_0 \left(1 - \dot{t}_{s,0}\right)\left(t - t_n - t_{s,n}\right)\right\} \tag{152}$$

which can be again further expanded to

$$x_R(t,n)=\frac{a_R}{a_T}\begin{pmatrix} x_0\left(\left(1-\dot{t}_{s,0}\right)\left(t-t_n-t_{c,n}-\left(t_{s,n}-t_{c,n}\right)\right),0\right) \\ \times\exp\left\{-j2\pi f_0\left(1-\dot{t}_{s,0}\right)\left(t_{s,n}-t_{c,n}\right)\right\} \\ \times\exp\left\{-j2\pi f_0\dot{t}_{s,0}\left(t-t_n-t_{c,n}\right)\right\} \\ \times\exp\left\{j2\pi f_0\left(t-t_n-t_{c,n}\right)\right\} \end{pmatrix}. \tag{153}$$

Once again, we mix this signal to baseband, digitally sample it, and expand to geometric parameters. However, we now keep Doppler scaling and yield

$$x_V(i,n)=\frac{a_R}{a_T}\begin{pmatrix} x_0\left(\left(1-\dot{t}_{s,0}\right)\left(T_{s,0}i-\frac{2}{c}\left(s_r+v_{sr}T_p n\right)\right),0\right) \\ \times\exp\left\{-j\frac{4\pi f_0}{c}\left(1-\dot{t}_{s,0}\right)s_r\right\} \\ \times\exp\left\{-j2\pi f_0\dot{t}_{s,0}T_{s,0}i\right\} \\ \times\exp\left\{-j\frac{4\pi f_0}{c}\left(1-\dot{t}_{s,0}\right)v_{sr}T_p n\right\} \end{pmatrix}. \tag{154}$$

Recall from earlier discussions that line two of this expression is essentially constant and can be ignored without detriment. In addition, $\dot{t}_{s,0}$ tends to be fairly small, allowing us to ignore it in the fourth line. Consequently the data model can be written as

$$x_V(i,n)\approx\frac{a_R}{a_T}\begin{pmatrix} x_0\left(\left(1-\dot{t}_{s,0}\right)\left(T_{s,0}i-\frac{2}{c}\left(s_r+v_{sr}T_p n\right)\right),0\right) \\ \times\exp\left\{-j2\pi f_0\dot{t}_{s,0}T_{s,0}i\right\} \\ \times\exp\left\{-j\frac{4\pi f_0}{c}v_{sr}T_p n\right\} \end{pmatrix}. \tag{155}$$

An IDFT across the Doppler index *n* can adequately resolve the velocity component v_{sr} and yield

$$y(i,u)\approx\frac{a_R}{a_T}\begin{pmatrix} x_0\left(\left(1-\dot{t}_{s,0}\right)\left(T_{s,0}i-\frac{2}{c}s_r\right),0\right) \\ \times\exp\left\{-j2\pi f_0\dot{t}_{s,0}T_{s,0}i\right\} \end{pmatrix}W_d\left(\frac{4\pi f_0}{c}T_p\left(\delta_{vr}u-v_{sr}\right)\right). \tag{156}$$

As before, this can in turn be used to estimate $\dot{t}_{s,0}$ which can be used to compensate the signal's carrier shift to yield

$$y'(i,u)=y(i,u)\exp\left\{j2\pi f_0\dot{t}_{s,n}T_{s,0}i\right\} \tag{157}$$

or

$$y'(i,u) \approx \frac{a_R}{a_T} x_0\left(\left(1-\dot{t}_{s,0}\right)\left(T_{s,0}i - \frac{2}{c}s_r\right),0\right) W_d\left(\frac{4\pi f_0}{c} T_p\left(\delta_{vr}u - v_{sr}\right)\right). \tag{158}$$

Note that the modulation is still scaled as a function of $\dot{t}_{s,0}$. As before, we have ignored migration in this model. If we continue to ignore migration, then we can compensate for the modulation dependence on $\dot{t}_{s,0}$ by adjusting the correlation based on the velocity estimate for v_{sr} for every Doppler index *u*. That is

$$z(k,u) \approx \text{xcorr}\left(\frac{x_0\left(\left(1-\dot{t}_{s,0}\right)T_{s,0}i,0\right)}{a_T}, y'(i,u)\right). \tag{159}$$

This is illustrated in Figure 7.

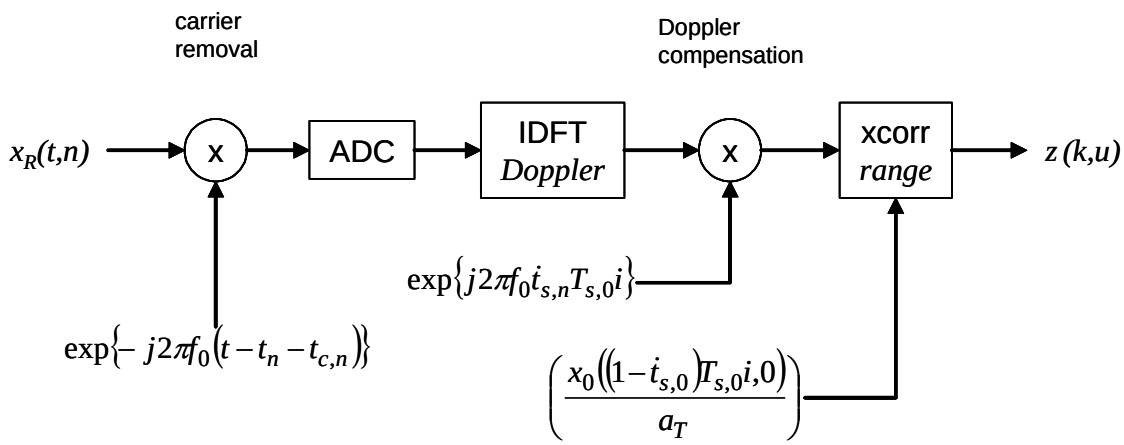

Figure 7. Range-Doppler processing with intra-pulse Doppler compensation but ignoring migration.

As before, mitigating migration can be achieved by somewhat more complex processing, by first undoing the Doppler IDFT, yielding

$$x'_V(i,n) \approx \frac{a_R}{a_T}\left(\begin{array}{l} x_0\left(\left(1-\dot{t}_{s,0}\right)\left(T_{s,0}i - \frac{2}{c}\left(s_r + v_{sr}T_p n\right)\right),0\right) \\ \times \exp\left\{-j\frac{4\pi f_0}{c}\left(v_{sr}T_p n\right)\right\} \end{array}\right). \tag{160}$$

We require entering the frequency domain of the modulation signal $x_0(t)$ by performing a DFT over index *i*, which yields

$$Y''(i',n) \approx \frac{a_R}{a_T}\left(\begin{array}{l}\frac{1}{(1-\dot{t}_{s,0})}X_0\left(\frac{df_0 i'}{(1-\dot{t}_{s,0})},0\right)\exp\left\{-j\frac{4\pi}{c}(s_r+v_{sr}T_p n)df_0 i'\right\}\\ \times\exp\left\{-j\frac{4\pi f_0}{c}(v_{sr}T_p n)\right\}\end{array}\right) \tag{161}$$

which can be rearranged to

$$Y''(i',n) \approx a_R\left(\begin{array}{l}\frac{1}{a_T(1-\dot{t}_{s,0})}X_0\left(\frac{df_0 i'}{(1-\dot{t}_{s,0})},0\right)\exp\left\{-j\frac{4\pi}{c}s_r df_0 i'\right\}\\ \times\exp\left\{-j\frac{4\pi f_0}{c}v_{sr}T_p\left(1+\frac{df_0}{f_0}i'\right)n\right\}\end{array}\right). \tag{162}$$

At this point we can multiply the data by the reference signal $X_0^*(df_0 i',0)/a_T$ to yield

$$Y'''(i',n) \approx a_R\left(\begin{array}{l}\frac{1}{a_T^2(1-\dot{t}_{s,0})}X_0^*(df_0 i',0)X_0\left(\frac{df_0 i'}{(1-\dot{t}_{s,0})},0\right)\exp\left\{-j\frac{4\pi}{c}s_r df_0 i'\right\}\\ \times\exp\left\{-j\frac{4\pi f_0}{c}v_{sr}T_p\left(1+\frac{df_0}{f_0}i'\right)n\right\}\end{array}\right). \tag{163}$$

Resampling such that

$$\left(1+\frac{df_0}{f_0}i'\right)n = n' \tag{164}$$

yields

$$Y'''(i',n') \approx a_R\left(\begin{array}{l}\frac{1}{a_T^2(1-\dot{t}_{s,0})}X_0^*(df_0 i',0)X_0\left(\frac{df_0 i'}{(1-\dot{t}_{s,0})},0\right)\exp\left\{-j\frac{4\pi}{c}s_r df_0 i'\right\}\\ \times\exp\left\{-j\frac{4\pi f_0}{c}v_{sr}T_p n'\right\}\end{array}\right) \tag{165}$$

or

$$Y'''(i',n') \approx a_R\left(\begin{array}{l}w_r(i')\exp\left\{-j\frac{4\pi}{c}s_r df_0 i'\right\}\\ \times\exp\left\{-j\frac{4\pi f_0}{c}v_{sr}T_p n'\right\}\end{array}\right)H_0(df_0 i',\dot{t}_{s,0}) \tag{166}$$

where

$$H_0\left(df_0 i', \dot{t}_{s,0}\right) = \frac{1}{\left(1-\dot{t}_{s,0}\right)}\left(\frac{X_0\left(\frac{df_0 i'}{\left(1-\dot{t}_{s,0}\right)}, 0\right)}{X_0\left(df_0 i', 0\right)}\right). \tag{167}$$

An IDFT across sample index n' yields

$$Y'''(i',u) \approx a_R\left(\begin{array}{l} w_r(i')\exp\left\{-j\frac{4\pi}{c}s_r df_0 i'\right\} \\ \times W_d\left(\frac{4\pi f_0}{c}T_p\left(\delta_{vr}u - v_{sr}\right)\right)\end{array}\right)H_0\left(df_0 i', \dot{t}_{s,0}\right). \tag{168}$$

With v_{sr} resolved, $\dot{t}_{s,0}$ is adequately estimated to allow compensation for $H_0\left(df_0 i', \dot{t}_{s,0}\right)$. This yields

$$Y''''(i',u) = Y'''(i',u)H_0^{-1}\left(df_0 i', \dot{t}_{s,0}\right) \tag{169}$$

or

$$Y''''(i',u) \approx a_R\left(w_r(i')\exp\left\{-j\frac{4\pi}{c}s_r df_0 i'\right\}\right)W_d\left(\frac{4\pi f_0}{c}T_p\left(\delta_{vr}u - v_{sr}\right)\right). \tag{170}$$

A remaining IDFT across range index i' completes the range-Doppler map target response and yields

$$z(k,u) = a_R W_r\left(\frac{4\pi df_0}{c}\left(\delta_r k - s_r\right)\right)W_d\left(\frac{4\pi f_0}{c}T_p\left(\delta_{vr}u - v_{sr}\right)\right). \tag{171}$$

These processing steps are illustrated in Figure 8.

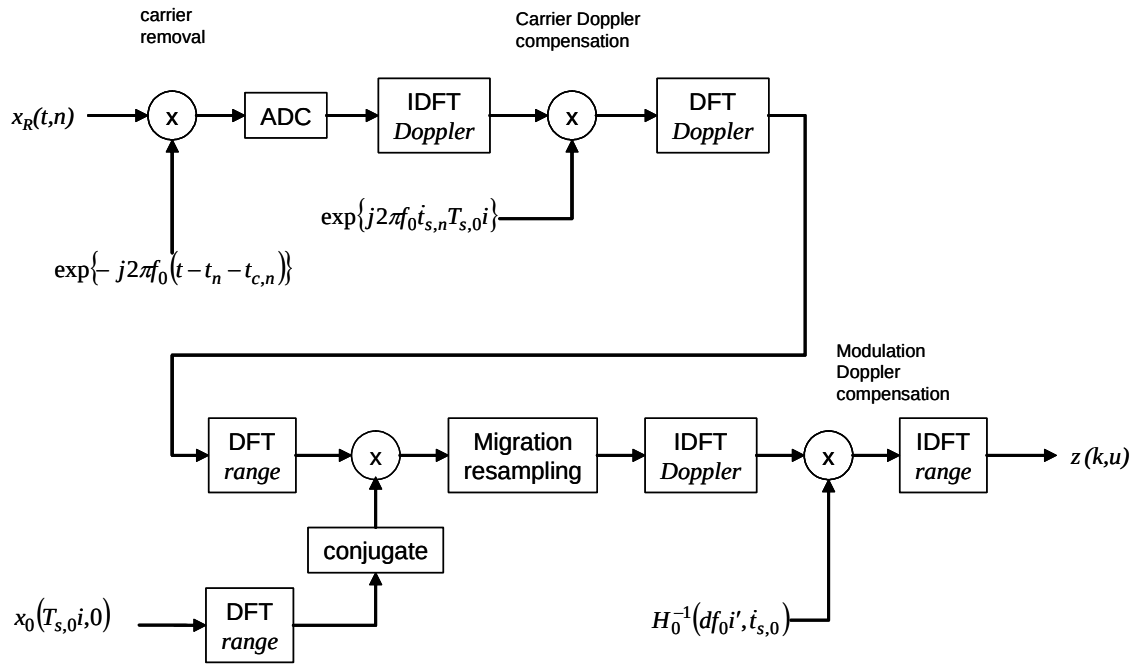

Figure 8. Range-Doppler processing with intra-pulse Doppler compensation and migration correction.

4.6 So What's the Point?

With range-Doppler processing of radar data, intra-pulse Doppler can be compensated and mitigated to a variety of degrees, even in the presence of range-Doppler migration. Consequently, a variety of waveforms (including NLFM waveforms) are usable to radar systems measuring target motion, such as coherent weather radar and MTI systems.

5 SAR Processing

We begin the discussion of image formation processing with the model for the received signal from a single distortionless isotropic point scatterer as

$$x_R(t,n) = \frac{a_R}{a_T} x_T\left(\left(1-\dot{t}_{s,n}\right)\left(t-t_n-t_{s,n}\right),n\right). \tag{172}$$

We shall furthermore assume the typical SAR model where the target scene is stationary and the radar moves, that is

$$r_{s,n} \approx r_{c,n} + \left(\cos\psi_{c,n}\cos\alpha_n s_y - \cos\psi_{c,n}\sin\alpha_n s_x\right) \tag{173}$$

or

$$r_{s,n} \approx r_{c,n} + \cos\psi_{c,n}\cos\alpha_n\left(s_y - \tan\alpha_n s_x\right) \tag{174}$$

We shall continue to presume that the energy spectrum for each pulse is real, band-limited, even, and centered at f_n.

5.1 SAR Processing – Negligible Intra-Pulse Doppler

In this section we employ frequency-domain filtering to implement the correlation of the received echo signal to ascertain range.

Assuming that intra-pulse Doppler is negligible, recall that the received signal can be simplified to

$$x_R(t,n) = \frac{a_R}{a_T} x_T\left(t-t_n-t_{s,n},n\right) \tag{175}$$

with spectrum

$$X_R(f,n) = \frac{a_R}{a_T} X_0(f-f_n,n)\exp\left\{-j2\pi t_{s,n} f\right\}. \tag{176}$$

We select as the delayed reference signal

$$x_m(t,n) = \frac{1}{a_T} x_T\left(\left(t-t_n-t_{c,n}\right),n\right) \tag{177}$$

with spectrum

$$X_m(f,n) = \frac{1}{a_T} X_0(f - f_n, n) \exp\{-j2\pi t_{c,n} f\}. \tag{178}$$

The Fourier Transform of an analog correlator output can then be expressed as

$$Y(f,n) = X_m^*(f,n) X_R(f,n). \tag{179}$$

This can be expanded to

$$Y(f,n) = \begin{pmatrix} \frac{1}{a_T} X_0^*(f - f_n, n) \exp\{j2\pi t_{c,n} f\} \\ \times \frac{a_R}{a_T} X_0(f - f_n, n) \exp\{-j2\pi t_{s,n} f\} \end{pmatrix} \tag{180}$$

and then simplified to

$$Y(f,n) = a_R \left[\frac{X_0^*(f - f_n, n)}{a_T} \frac{X_0(f - f_n, n)}{a_T} \right] \exp\{-j2\pi (t_{s,n} - t_{c,n}) f\}. \tag{181}$$

This can be rewritten as

$$Y(f,n) = a_R \left| \frac{X_0(f - f_n, n)}{a_T} \right|^2 \exp\{-j2\pi (t_{s,n} - t_{c,n}) f\} \tag{182}$$

If the original signals had been sampled, and their Fourier Transforms calculated with a Discrete Fourier Transform (DFT), then we would have samples at discrete frequencies given by

$$f = f_n + df_n \, i \tag{183}$$

where

f_n = the center frequency of pulse n,
df_n = the frequency sample increment for pulse n, and
i = the frequency index, $-I/2 \le i < I/2$. (184)

Note that the sampling parameters of each pulse are in fact pulse-specific. This can be achieved either by using an agile sampling circuit, or by using a fixed sampling strategy and then digitally resampling the data using signal processing techniques. In either case, we will presume that samples are obtained with correct ultimate positions, whatever we require those ultimately positions to be.

The digital correlator output signal spectrum would be

$$Y(i,n) = a_R \left| \frac{X_0(df_n\, i,n)}{a_T} \right|^2 \exp\{-j2\pi(t_{s,n} - t_{c,n})(f_n + df_n\, i)\}. \tag{185}$$

Observe that once again the magnitude-squared of the transmit-signal spectrum now constitutes a positive real-valued weighting function, behaving like a window or aperture weighting function, thereby influencing the shape of the ultimate range impulse response of the radar. We simplify this expression somewhat by identifying the equivalent weighting function explicitly as

$$w_r(i,n) = \left| \frac{X_0(df_n\, i,n)}{a_T} \right|^2 . \tag{186}$$

Incorporating geometric definitions into this, and rearranging a bit yields

$$Y(i,n) = a_R w_r(i,n) \exp\left\{ -j\frac{4\pi f_n}{c}\left(1 + \frac{df_n}{f_n}\, i\right) \cos\psi_{c,n} \cos\alpha_n (s_y - s_x \tan\alpha_n) \right\} \tag{187}$$

which can be further rearranged to

$$Y(i,n) = a_R \left[\begin{array}{l} w_r(i,n) \exp\left\{ -j\frac{4\pi df_n}{c} \cos\psi_{c,n} \cos\alpha_n s_y i \right\} \\ \times \exp\left\{ +j\frac{4\pi f_n}{c}\left(1 + \frac{df_n}{f_n}\, i\right) \cos\psi_{c,n} \cos\alpha_n (s_x \tan\alpha_n) \right\} \\ \times \exp\left\{ -j\frac{4\pi f_n}{c} \cos\psi_{c,n} \cos\alpha_n s_y \right\} \end{array} \right] . \tag{188}$$

We now choose specific values

$$f_n = \left(\frac{\cos\psi_{c,0}}{\cos\psi_{c,n} \cos\alpha_n} \right) f_0 \tag{189}$$

and

$$df_n = \left(\frac{\cos\psi_{c,0}}{\cos\psi_{c,n} \cos\alpha_n} \right) df_0 \tag{190}$$

for some constant nominal values f_0 and df_0. This allows the simplification

$$Y(i,n) = a_R \begin{bmatrix} w_r(i,n)\exp\left\{-j\dfrac{4\pi d f_0 \cos\psi_{c,0}}{c} s_y i\right\} \\ \times \exp\left\{+j\dfrac{4\pi f_0 \cos\psi_{c,0}}{c} s_x \left(1+\dfrac{d f_0}{f_0} i\right)\tan\alpha_n\right\} \\ \times \exp\left\{-j\dfrac{4\pi f_0 \cos\psi_{c,0}}{c} s_y\right\} \end{bmatrix}. \tag{191}$$

Several comments are in order.

- The third line in the square brackets is inconsequential to ascertaining range and azimuth location of the target point, and hence can be ignored.
- The second line in the square brackets has phase linear in $\tan\alpha_n$, suggesting processing across α_n to ascertain s_x.
- The second line in the square brackets has phase also with a dependence on index *i*, which suggests undesirable migration if left unmitigated.
- The first term in the square brackets has phase linear in index *i*, suggesting an IDFT to ascertain s_r.
- The weighting function $w_r(i,n)$ is effectively applied by virtue of the transmit waveform characteristics. Its principal effect is in the range direction, along index *i*. While a subtle effect also exists in the azimuth direction, along index *n*, it is of little consequence and can generally be ignored. Consequently we can approximate

  $$w_r(i,n) \approx w_r(i,0). \tag{192}$$

- Any mitigation of sidelobes as a result of processing across index *n* will require additional overt weighting or filtering applied.

If we ignore migration effects, then we need to sample at, or resample to,

$$\tan\alpha_n = d\alpha\, n \tag{193}$$

where

$$d\alpha \text{ = nominal azimuth sample spacing factor.} \tag{194}$$

To mitigate migration, we need to use a combination of sampling and resampling to effect

$$\left(1+\frac{df_0}{f_0}\,i\right)\tan\alpha_n = d\alpha\, n'\,. \tag{195}$$

This allows us to write a migration corrected model as

$$Y(i,n') \approx a_R \left[\begin{array}{l} w_r(i,0)\exp\left\{-\,j\,\dfrac{4\pi d f_0\cos\psi_{c,0}}{c}\,s_y i\right\} \\ \times\exp\left\{+\,j\,\dfrac{4\pi f_0\cos\psi_{c,0}}{c}\,s_x\, d\alpha\, n'\right\} \end{array}\right]. \tag{196}$$

An IDFT applied over index i, and DFT applied over indices n' will yield the range-Doppler map target response described by

$$z(k,u) = a_R W_r\left(-\frac{4\pi d f_0\cos\psi_{c,0}}{c}\,s_y + \frac{2\pi}{K}k\right) W_d\left(\frac{4\pi f_0 d\alpha\cos\psi_{c,0}}{c}\,s_x - \frac{2\pi}{U}u\right) \tag{197}$$

which can be rewritten in the form

$$z(k,u) = a_R W_r\left(\frac{4\pi\, d f_0\cos\psi_{c,0}}{c}\left(\delta_y k - s_y\right)\right) W_d\left(\frac{4\pi f_0 d\alpha\cos\psi_{c,0}}{c}\left(\delta_x u - s_x\right)\right). \tag{198}$$

where

δ_y = the sample spacing for range location s_y, and

δ_x = the sample spacing for azimuth location s_x. (199)

We note that the combination of choosing the specific nature of f_n and df_n, coupled with choosing sample locations at $d\alpha\, n'$ to mitigate migration, constitute placing data samples onto a rectangular grid in the Fourier space of the scene. These are the essential steps for the Polar Format Algorithm (PFA) for SAR image formation. PFA is a popular technique for fine resolution SAR image formation first developed by Walker.[19] It is typically applied to data collected with an LFM waveform and stretch processing.[20] We have assumed neither LFM waveforms, nor stretch processing in our development. Clearly PFA can be employed for waveforms other than LFM chirps.

The processing steps are illustrated in Figure 9.

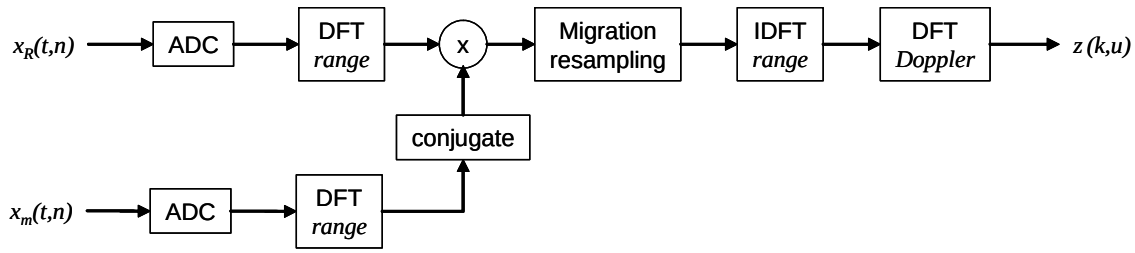

Figure 9. Frequency-domain processing with migration correction.

5.2 SAR Processing – Uniform Intra-Pulse Doppler

In this section we again employ frequency-domain filtering to implement the correlation of the received echo signal to ascertain range.

Assuming that intra-pulse Doppler is no longer negligible, recall that the received signal can be simplified to

$$x_R(t,n) = \frac{a_R}{a_T} x_T\left(\left(1-\dot{t}_{s,n}\right)\left(t-t_n-t_{s,n}\right),n\right). \tag{200}$$

Recall that for a wide variety of SAR applications, the variation of intra-pulse Doppler within the scene being imaged is sufficiently limited that intra-pulse Doppler scaling can be presumed to be uniform in the image. Consequently for this development we may presume

$$\dot{t}_{s,n} \approx \dot{t}_{c,n}. \tag{201}$$

which leads to

$$x_R(t,n) \approx \frac{a_R}{a_T} x_T\left(\left(1-\dot{t}_{c,n}\right)\left(t-t_n-t_{s,n}\right),n\right). \tag{202}$$

with spectrum

$$X_R(f,n) \approx \frac{a_R/a_T}{\left(1-\dot{t}_{c,n}\right)} X_0\left(\frac{f}{\left(1-\dot{t}_{c,n}\right)} - f_n, n\right) \exp\left\{-j2\pi t_{s,n} f\right\}. \tag{203}$$

We select as the delayed reference signal

$$x_m(t,n) = \frac{1}{a_T} x_T\left(\left(1-\dot{t}_{c,n}\right)\left(t-t_n-t_{c,n}\right),n\right) \tag{204}$$

with spectrum

$$X_m(f,n) = \frac{1/a_T}{(1-\dot{t}_{c,n})} X_0\left(\frac{f}{(1-\dot{t}_{c,n})} - f_n, n\right) \exp\{-j2\pi t_{c,n} f\}. \tag{205}$$

The Fourier Transform of an analog correlator output can then be expressed as

$$Y(f,n) = X_m^*(f,n) X_R(f,n). \tag{206}$$

This can be expanded to

$$Y(f,n) \approx \left(\begin{array}{l} \frac{1/a_T}{(1-\dot{t}_{c,n})} X_0^*\left(\frac{f}{(1-\dot{t}_{c,n})} - f_n, n\right) \exp\{j2\pi t_{c,n} f\} \\ \times \frac{a_R/a_T}{(1-\dot{t}_{c,n})} X_0\left(\frac{f}{(1-\dot{t}_{c,n})} - f_n, n\right) \exp\{-j2\pi t_{s,n} f\} \end{array} \right) \tag{207}$$

and then simplified to

$$Y(f,n) \approx a_R \left[\frac{X_0^*\left(\frac{f}{(1-\dot{t}_{c,n})} - f_n, n\right)}{a_T(1-\dot{t}_{c,n})} \frac{X_0\left(\frac{f}{(1-\dot{t}_{c,n})} - f_n, n\right)}{a_T(1-\dot{t}_{c,n})} \right] \exp\{-j2\pi(t_{s,n} - t_{c,n}) f\}. \tag{208}$$

This can be rewritten as

$$Y(f,n) \approx a_R \left| \frac{X_0\left(\frac{f}{(1-\dot{t}_{c,n})} - f_n, n\right)}{a_T(1-\dot{t}_{c,n})} \right|^2 \exp\{-j2\pi(t_{s,n} - t_{c,n}) f\}. \tag{209}$$

As in the preceding section, the quantity in the magnitude bars is still a weighting function, primarily in the *f* direction, however it is shifted and scaled slightly by the intra-pulse Doppler. For small line of sight velocities (small intra-pulse Doppler), this can probably be henceforth ignored to negligible consequence. This would allow the approximation

$$\left|\frac{X_0\left(\frac{f}{\left(1-\dot{t}_{c,n}\right)}-f_n,n\right)}{a_T\left(1-\dot{t}_{c,n}\right)}\right|^2 \approx \left|\frac{X_0\left(f-f_n,n\right)}{a_T}\right|^2 \tag{210}$$

and allow subsequent processing to continue as detailed in the preceding section.

However, if we choose to not make this assumption, then the processing can proceed with slight modification. The amplitude scaling by $\left(1-\dot{t}_{c,n}\right)$ is for practical purposes inconsequential. Therefore, the data model can then be simplified to

$$Y\left(f,n\right) \approx a_R \left|\frac{X_0\left(\frac{f}{\left(1-\dot{t}_{c,n}\right)}-f_n,n\right)}{a_T}\right|^2 \exp\left\{-j2\pi\left(t_{s,n}-t_{c,n}\right)f\right\}. \tag{211}$$

By combinations of sampling and resampling, we choose data samples at frequency locations

$$f = \left(1-\dot{t}_{c,n}\right)\left(f_n + df_n\, i\right) \tag{212}$$

Note that as in the preceding section the sampling parameters of each pulse are in fact pulse-specific. The digital correlator output signal spectrum would then be

$$Y\left(i,n\right) \approx a_R \left|\frac{X_0\left(df_n\, i,n\right)}{a_T}\right|^2 \exp\left\{-j2\pi\left(t_{s,n}-t_{c,n}\right)\left(1-\dot{t}_{c,n}\right)\left(f_n + df_n\, i\right)\right\}. \tag{213}$$

Observe that once again the magnitude-squared of the transmit-signal spectrum now constitutes a positive real-valued weighting function, behaving like a window or aperture weighting function, thereby influencing the shape of the ultimate range impulse response of the radar. We again simplify this expression somewhat by identifying the equivalent weighting function explicitly as

$$w_r\left(i,n\right) = \left|\frac{X_0\left(df_n\, i,n\right)}{a_T}\right|^2 . \tag{214}$$

Incorporating geometric definitions into this, and rearranging a bit yields

$$Y(i,n) \approx a_R w_r(i,n) \exp\left\{ -j \frac{4\pi f_n}{c} \left(1 + \frac{df_n}{f_n} i \right) \left(1 - \dot{t}_{c,n}\right) \cos\psi_{c,n} \cos\alpha_n \left(s_y - s_x \tan\alpha_n\right) \right\}$$

(215)

which can be further rearranged to

$$Y(i,n) \approx a_R \left[\begin{array}{l} w_r(i,n) \exp\left\{ -j \frac{4\pi df_n}{c} \left(1 - \dot{t}_{c,n}\right) \cos\psi_{c,n} \cos\alpha_n s_y i \right\} \\ \times \exp\left\{ +j \frac{4\pi f_n}{c} \left(1 + \frac{df_n}{f_n} i \right) \left(1 - \dot{t}_{c,n}\right) \cos\psi_{c,n} \cos\alpha_n \left(s_x \tan\alpha_n\right) \right\} \\ \times \exp\left\{ -j \frac{4\pi f_n}{c} \left(1 - \dot{t}_{c,n}\right) \cos\psi_{c,n} \cos\alpha_n s_y \right\} \end{array} \right]. \quad (216)$$

We now choose specific values for each pulse

$$f_n = \left(\frac{\cos\psi_{c,0}}{\cos\psi_{c,n} \cos\alpha_n \left(1 - \dot{t}_{c,n}\right)} \right) f_0 \quad (217)$$

and

$$df_n = \left(\frac{\cos\psi_{c,0}}{\cos\psi_{c,n} \cos\alpha_n \left(1 - \dot{t}_{c,n}\right)} \right) df_0 \quad (218)$$

for some constant nominal values f_0 and df_0. This allows the simplification

$$Y(i,n) \approx a_R \left[\begin{array}{l} w_r(i,n) \exp\left\{ -j \frac{4\pi df_0 \cos\psi_{c,0}}{c} s_y i \right\} \\ \times \exp\left\{ +j \frac{4\pi f_0 \cos\psi_{c,0}}{c} s_x \left(1 + \frac{df_0}{f_0} i \right) \tan\alpha_n \right\} \\ \times \exp\left\{ -j \frac{4\pi f_0 \cos\psi_{c,0}}{c} s_y \right\} \end{array} \right]. \quad (219)$$

This is now in the same form as in the preceding section, and can be henceforth processed in the same manner to achieve

$$z(k,u) = a_R W_r\left(\frac{4\pi\, df_0 \cos\psi_{c,0}}{c} \left(\delta_y k - s_y\right) \right) W_d\left(\frac{4\pi f_0 d\alpha \cos\psi_{c,0}}{c} \left(\delta_x u - s_x\right) \right). \quad (220)$$

Consequently, the effect of a uniform intra-pulse Doppler scaling is to shift the center frequency and scale the bandwidth of the received echo. We have shown that this can be accommodated by adjusting the image formation processing with scaled frequency factors f_n and df_n. This effectively perturbs the matched filter to be matched to the Doppler scaled echoes.

The processing steps are the same as illustrated in Figure 9.

5.3 SAR Processing – Intra-Pulse Doppler Variations

In this section we build on the results of the previous section but now incorporate intra-pulse Doppler that varies excessively across the scene being imaged, that is, even if compensated to the scene center, still exhibits intolerable effects at the scene edges.

Recall that the received signal can be modeled as

$$x_R(t,n) = \frac{a_R}{a_T} x_T\left(\left(1-\dot{t}_{s,n}\right)\left(t-t_n-t_{s,n}\right),n\right). \tag{221}$$

with spectrum

$$X_R(f,n) \approx \frac{a_R/a_T}{\left(1-\dot{t}_{s,n}\right)} X_0\left(\frac{f}{\left(1-\dot{t}_{s,n}\right)} - f_n, n\right)\exp\left\{-j2\pi t_{s,n} f\right\}. \tag{222}$$

We select as the delayed reference signal

$$x_m(t,n) = \frac{1}{a_T} x_T\left(\left(1-\dot{t}_{c,n}\right)\left(t-t_n-t_{c,n}\right),n\right) \tag{223}$$

with spectrum

$$X_m(f,n) = \frac{1/a_T}{\left(1-\dot{t}_{c,n}\right)} X_0\left(\frac{f}{\left(1-\dot{t}_{c,n}\right)} - f_n, n\right)\exp\left\{-j2\pi t_{c,n} f\right\}. \tag{224}$$

The Fourier Transform of an analog correlator output can then be expanded to

$$Y(f,n) \approx \left(\begin{array}{l} \frac{1/a_T}{\left(1-\dot{t}_{c,n}\right)} X_0^*\left(\frac{f}{\left(1-\dot{t}_{c,n}\right)} - f_n, n\right)\exp\left\{j2\pi t_{c,n} f\right\} \\ \times \frac{a_R/a_T}{\left(1-\dot{t}_{s,n}\right)} X_0\left(\frac{f}{\left(1-\dot{t}_{s,n}\right)} - f_n, n\right)\exp\left\{-j2\pi t_{s,n} f\right\} \end{array}\right) \tag{225}$$

and then simplified to

$$Y(f,n) \approx a_R \left[\frac{X_0^*\left(\frac{f}{\left(1-\dot{t}_{c,n}\right)} - f_n, n \right)}{a_T\left(1-\dot{t}_{c,n}\right)} \frac{X_0\left(\frac{f}{\left(1-\dot{t}_{s,n}\right)} - f_n, n \right)}{a_T\left(1-\dot{t}_{s,n}\right)} \right] \exp\left\{ -j2\pi\left(t_{s,n} - t_{c,n}\right) f \right\}. \tag{226}$$

We now define the difference

$$\dot{t}_{sc,n} = \dot{t}_{s,n} - \dot{t}_{c,n}. \tag{227}$$

The data model can then be rewritten as

$$Y(f,n) \approx \left[\begin{array}{l} a_R \left| \frac{X_0\left(\frac{f}{\left(1-\dot{t}_{c,n}\right)} - f_n, n \right)}{a_T\left(1-\dot{t}_{c,n}\right)} \right|^2 \exp\left\{ -j2\pi\left(t_{s,n} - t_{c,n}\right) f \right\} \\ \times H_{IPD}\left(\frac{f}{\left(1-\dot{t}_{c,n}\right)} - f_n, \dot{t}_{sc,n} \right) \end{array} \right] \tag{228}$$

where the residual effects of intra-pulse Doppler variations are embodied in a perturbation filter

$$H_{IPD}\left(\frac{f}{\left(1-\dot{t}_{c,n}\right)} - f_n, \dot{t}_{sc,n} \right) = \left(\frac{1-\dot{t}_{c,n}}{1-\dot{t}_{s,n}} \right) \frac{X_0\left(\frac{f}{\left(1-\dot{t}_{c,n}-\dot{t}_{sc,n}\right)} - f_n, n \right)}{X_0\left(\frac{f}{\left(1-\dot{t}_{c,n}\right)} - f_n, n \right)}. \tag{229}$$

As before, the amplitude scaling by $\left(1-\dot{t}_{c,n}\right)$ and $\left(1-\dot{t}_{s,n}\right)$ is for practical purposes inconsequential. Therefore, the data model can be simplified to

$$Y(f,n) \approx \left[\begin{array}{l} a_R \left| \frac{X_0\left(\frac{f}{\left(1-\dot{t}_{c,n}\right)} - f_n, n \right)}{a_T} \right|^2 \exp\left\{ -j2\pi\left(t_{s,n} - t_{c,n}\right) f \right\} \\ \times H_{IPD}\left(\frac{f}{\left(1-\dot{t}_{c,n}\right)} - f_n, \dot{t}_{sc,n} \right) \end{array} \right] \tag{230}$$

where

$$H_{IPD}\left(\frac{f}{\left(1-\dot{t}_{c,n}\right)}-f_n,\dot{t}_{sc,n}\right)\approx\frac{X_0\left(\frac{f}{\left(1-\dot{t}_{c,n}\right)}-f_n+\dot{t}_{sc,n}f,n\right)}{X_0\left(\frac{f}{\left(1-\dot{t}_{c,n}\right)}-f_n,n\right)}. \tag{231}$$

By combinations of sampling and resampling, we again choose data samples at frequency locations

$$f=\left(1-\dot{t}_{c,n}\right)\left(f_n+df_n\ i\right) \tag{232}$$

Note that as in the preceding section the sampling parameters of each pulse are in fact pulse-specific. The digital correlator output signal spectrum would then be

$$Y(i,n)\approx\left[\begin{array}{l} a_R\left|\frac{X_0\left(df_n\ i,n\right)}{a_T}\right|^2\exp\left\{-j2\pi\left(t_{s,n}-t_{c,n}\right)\left(1-\dot{t}_{c,n}\right)\left(f_n+df_n\ i\right)\right\} \\ \times H_{IPD}\left(df_n\ i,\dot{t}_{sc,n}\right)\end{array}\right]. \tag{233}$$

Observe that once again the magnitude-squared of the transmit-signal spectrum now constitutes a positive real-valued weighting function, behaving like a window or aperture weighting function, thereby influencing the shape of the ultimate range impulse response of the radar. We again simplify this expression somewhat by identifying the equivalent weighting function explicitly as

$$w_r(i,n)=\left|\frac{X_0\left(df_n\ i,n\right)}{a_T}\right|^2. \tag{234}$$

Incorporating geometric definitions into this, and rearranging a bit yields

$$Y(i,n)\approx\left[\begin{array}{l} a_R w_r(i,n) \\ \times\exp\left\{-j\frac{4\pi f_n}{c}\left(1+\frac{df_n}{f_n}\ i\right)\left(1-\dot{t}_{c,n}\right)\cos\psi_{c,n}\cos\alpha_n\left(s_y-s_x\tan\alpha_n\right)\right\} \\ \times H_{IPD}\left(df_n\ i,\dot{t}_{sc,n}\right)\end{array}\right] \tag{235}$$

which can be further rearranged to

$$Y(i,n) \approx a_R \begin{bmatrix} w_r(i,n)\exp\left\{-j\frac{4\pi df_n}{c}\left(1-\dot{t}_{c,n}\right)\cos\psi_{c,n}\cos\alpha_n s_y i\right\} \\ \times\exp\left\{+j\frac{4\pi f_n}{c}\left(1+\frac{df_n}{f_n}i\right)\left(1-\dot{t}_{c,n}\right)\cos\psi_{c,n}\cos\alpha_n\left(s_x\tan\alpha_n\right)\right\} \\ \times\exp\left\{-j\frac{4\pi f_n}{c}\left(1-\dot{t}_{c,n}\right)\cos\psi_{c,n}\cos\alpha_n s_y\right\} \\ \times H_{IPD}\left(df_n\ i,\dot{t}_{sc,n}\right) \end{bmatrix}. \quad (236)$$

We again choose specific values for each pulse

$$f_n = \kappa_n f_0 \quad (237)$$

and

$$df_n = \kappa_n df_0 \quad (238)$$

where

$$\kappa_n = \frac{\cos\psi_{c,0}}{\cos\psi_{c,n}\cos\alpha_n\left(1-\dot{t}_{c,n}\right)} \quad (239)$$

for some constant nominal values f_0 and df_0. This allows the simplification

$$Y(i,n) \approx a_R \begin{bmatrix} w_r(i,n)\exp\left\{-j\frac{4\pi df_0\cos\psi_{c,0}}{c}s_y i\right\} \\ \times\exp\left\{+j\frac{4\pi f_0\cos\psi_{c,0}}{c}s_x\left(1+\frac{df_0}{f_0}i\right)\tan\alpha_n\right\} \\ \times\exp\left\{-j\frac{4\pi f_0\cos\psi_{c,0}}{c}s_y\right\} \\ \times H_{IPD}\left(\kappa_n df_0\ i,\dot{t}_{sc,n}\right) \end{bmatrix}. \quad (240)$$

A closer examination of $H_{IPD}\left(\kappa_n df_0\ i,\dot{t}_{sc,n}\right)$ identifies

$$H_{IPD}\left(\kappa_n df_0\ i,\dot{t}_{sc,n}\right) \approx \frac{X_0\left(\kappa_n df_0\ i+\dot{t}_{sc,n}\kappa_n\left(1-\dot{t}_{c,n}\right)\left(f_0+df_0\ i\right),n\right)}{X_0\left(\kappa_n df_0\ i,n\right)}. \quad (241)$$

From preceding discussion, we recall that $\dot{t}_{sc,n}$ is relatively small, and can often be presumed to be negligible. However in this development we have assumed that $\dot{t}_{sc,n}$ is sufficiently significant that it needs to be compensated. Nevertheless, effective

mitigation may be expected even if it is only approximately compensated. To that end, we assume that for $H_{IPD}\left(\kappa_n df_0\ i, \dot{t}_{sc,n}\right)$

$$\begin{aligned}
&\kappa_n \approx 1, \\
&\left(1-\dot{t}_{c,n}\right) \approx 1, \\
&\left(f_0 + df_0\ i\right) \approx f_0, \text{ and} \\
&\dot{t}_{sc,n} \approx \dot{t}_{sc,0}.
\end{aligned} \tag{242}$$

such that for our purposes

$$H_{IPD}\left(\kappa_n df_0\ i, \dot{t}_{sc,n}\right) \approx H_{IPD}\left(df_0\ i, \dot{t}_{sc,0}\right) \approx \frac{X_0\left(df_0\ i + \dot{t}_{sc,0} f_0, 0\right)}{X_0\left(df_0\ i, 0\right)}. \tag{243}$$

This has removed the dependence of the perturbation filter on index *n*. Furthermore, it now depends only on sampling index *i* and intra-pulse Doppler difference $\dot{t}_{sc,0}$.

Continuing with the processing, ignoring constant phase terms, ignoring minor azimuth tapering, and resampling to mitigate migration yields

$$Y(i,n') \approx a_R \begin{bmatrix} w_r(i,0)\exp\left\{-j\dfrac{4\pi df_0 \cos\psi_{c,0}}{c} s_y i\right\} \\ \times \exp\left\{+j\dfrac{4\pi f_0 \cos\psi_{c,0}}{c} s_x\, d\alpha\, n'\right\} \\ \times H_{IPD}\left(df_0\ i, \dot{t}_{sc,0}\right) \end{bmatrix}. \tag{244}$$

A DFT along azimuth index n' yields

$$Y(i,u) \approx a_R \begin{bmatrix} w_r(i,0)\exp\left\{-j\dfrac{4\pi df_0 \cos\psi_{c,0}}{c} s_y i\right\} \\ \times W_d\left(\dfrac{4\pi f_0 d\alpha \cos\psi_{c,0}}{c}\left(\delta_x u - s_x\right)\right) \\ \times H_{IPD}\left(df_0\ i, \dot{t}_{sc,0}\right) \end{bmatrix}. \tag{245}$$

At this point we have resolved target location s_x corresponding to range-Doppler map position $\delta_x u$. This allows a corresponding estimate for $\dot{t}_{sc,0}$ for each position $\delta_x u$ via

$$\dot{t}_{sc,0} \approx v_{aircraft} \sin\varphi \frac{s_x}{r_{c,0}} \delta_x u \,. \tag{246}$$

As a consequence, we can compensate for the perturbation filter by calculating for each azimuth position

$$Y'(i,u) = Y(i,u) H_{IPD}^{-1}\left(df_0\ i, \dot{t}_{sc,0}\right) \tag{247}$$

which yields

$$Y'(i,u) \approx a_R \begin{bmatrix} w_r(i,0)\exp\left\{-j\dfrac{4\pi d f_0 \cos\psi_{c,0}}{c} s_y i\right\} \\ \times W_d\left(\dfrac{4\pi f_0 d\alpha \cos\psi_{c,0}}{c}\left(\delta_x u - s_x\right)\right) \end{bmatrix}. \tag{248}$$

A subsequent IDFT across index i then yields the same output as in previous sections, namely

$$z(k,u) = a_R W_r\left(\frac{4\pi\, d f_0 \cos\psi_{c,0}}{c}\left(\delta_y k - s_y\right)\right) W_d\left(\frac{4\pi f_0 d\alpha \cos\psi_{c,0}}{c}\left(\delta_x u - s_x\right)\right). \tag{249}$$

Essentially, we have employed the process of the previous section, but with an added correction step after final azimuth processing, but before final range processing. This is illustrated in Figure 10.

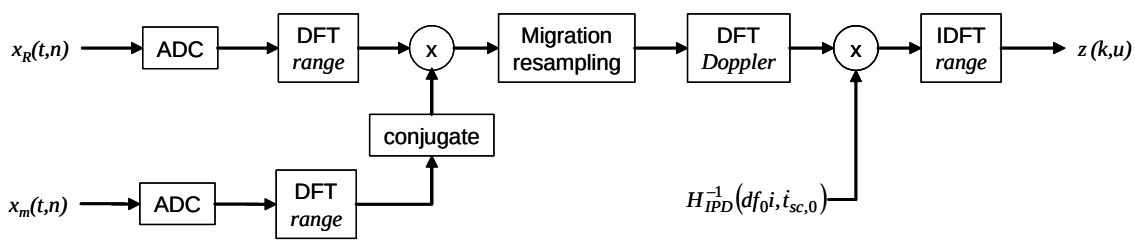

Figure 10. SAR processing for intra-pulse Doppler variations within the scene.

5.4 Stretch Processing

Stretch processing was first proposed by Caputi. Its essence is in the realization that if a LFM signal is “de-chirped” or “de-ramped” then the original signal’s matched filter degenerates into a Fourier Transform of the de-chirped result. This is only strictly true for LFM waveforms. No similar techniques for NLFM waveforms have been reported in the literature. Further study of stretch processing for NLFM waveforms is currently underway, but is beyond the scope of this report.

5.5 So What’s the Point?

With SAR processing, intra-pulse Doppler can be compensated and mitigated to a variety of degrees, even in the presence of range-Doppler migration. Consequently, a variety of waveforms (including NLFM waveforms) are usable for SAR processing, including high-performance algorithms like the Polar Format Algorithm.

6 Conclusions

The following principal conclusions should be drawn from this report.

With range-Doppler processing of radar data, using either LFM or NLFM waveforms, intra-pulse Doppler can be compensated and mitigated to a variety of degrees, even in the presence of range-Doppler migration.

Consequently, a variety of waveforms (including NLFM waveforms) are readily usable to radar systems measuring target motion, such as coherent weather radar and MTI systems, and for SAR processing, including high-performance algorithms like the Polar Format Algorithm.

NLFM waveforms are simply designed, easily produced, and readily processed for high-performance radar applications. Doing so will yield a 1-2 dB advantage in SNR over LFM waveforms if processing sidelobes need to be controlled.

“The world hates change, yet it is the only thing that has brought progress.”

Charles Kettering

REFERENCES

[1] A. W. Doerry, "Performance Limits for Synthetic Aperture Radar – second edition", Sandia Report SAND2006-0821, Unlimited Release, February 2006.

[2] A. W. Doerry, "Generating Nonlinear FM Chirp Waveforms for Radar", Sandia Report SAND2006-5856, Unlimited Release, September 2006.

[3] E. Fowle, "The design of FM pulse compression signals", *IEEE Transactions on Information Theory*, Vol. 10 , Issue 1, pp. 61–67, Jan 1964.

[4] Byron M. Keel, Jay A. Saffold, Mark R. Waibridge, and John Chadwick, "Non-linear stepped chirp waveforms with sub-pulse processing for range sidelobe suppression", SPIE Conference on Radar Sensor Technoloqy III, Vol. 3395, pp 87-98, Orlando, Florida, April 1998.

[5] J. A. Johnston, "Analysis of the pulse compression of Doppler shifted nonlinear frequency modulated signals", Electronics Letters, vol. 20, no. 25-26, pp. 1054-5, 6 Dec. 1984.

[6] R. J. Keeler, C. A. Hwang, "Pulse compression for weather radar", Proceedings of the IEEE 1995 International Radar Conference, pp. 529-35, Alexandria, VA, USA, 8-11 May 1995.

[7] H.D. Griffiths and L. Vinagre, "Design of low-sidelobe pulse compression waveforms", Electronics Letters, vol. 30, no. 12, pp.1004-5, 9 June 1994.

[8] D. P. Morgan, "Nonlinear chirp radar waveforms with improved tolerance to Doppler shifts", IEE Colloquium on `Physics and Device Applications of Acoustic Waves' (Digest No.69), p. 8/1-5, London, UK, 22 May 1987.

[9] T. Collins, P. Atkins, "Nonlinear frequency modulation chirps for active sonar", IEE Proceedings - Radar, Sonar and Navigation, vol. 146, no. 6, pp. 312-16, Dec. 1999.

[10] J. A. Johnston, A. C. Fairhead, "Waveform design and Doppler sensitivity analysis for nonlinear FM chirp pulses", IEE Proceedings F (Communications, Radar and Signal Processing), Vol. 133, No. 2, p. 163-175, April 1986.

[11] A. W. Rihaczek, "Doppler-tolerant signal waveforms", *Proceedings of the IEEE*, Vol. 54, Issue 6, pp. 849 – 857, June 1966.

[12] H. Urkowitz, N. J. Bucci, “Doppler Tolerant Range Sidelobe Suppression for Meteorological Radar With Pulse-Compression”, Proceedings of the 1992 International Geoscience and Remote Sensing Symposium, IGARSS '92, Vol. 1, pp. 206-208, Houston, TX, May 26-29, 1992.

[13] M. B. N. Butler, “Radar applications of s.a.w. dispersive filters”, IEE Proceedings F (Communications, Radar and Signal Processing), vol. 127, no. 2, pp. 118-24, April 1980.

[14] M. I. Skolnik, *Introduction to Radar Systems*, second edition, ISBN 0-07-057909-1, McGraw-Hill, Inc., 1980

[15] John C. Curlander, Robert N. McDonough, *Synthetic Aperture Radar, Systems & Signal Processing*, ISBN 0-471-85770-X, John Wiley & Sons, 1991.

[16] R. C. DiPietro, R. P. Perry, R. L. Fante, “SAR imaging and detection of moving targets”, Proceedings of the SPIE - The International Society for Optical Engineering, Algorithms for Synthetic Aperture Radar Imagery V , vol. 3370, pp. 73-84, Orlando, FL, USA, 14-17 April 1998.

[17] R. P. Perry, R. C. DiPietro, R. L. Fante, “SAR imaging of moving targets”, *IEEE Transactions on Aerospace and Electronic Systems*, vol. 35, no. 1, pp. 188-200, Jan. 1999.

[18] R. C. DiPietro, R. L. Fante, R. P. Perry, “Imaging of moving targets using synthetic aperture radar”, IEEE Antennas and Propagation Society International Symposium 1997, Digest (Cat. No.97CH36122), vol. 4, pp. 2590-2, Montreal, Que., Canada, 13-18 July 1997.

[19] J. L. Walker, “Range-Doppler Imaging of Rotating Objects,” *IEEE Trans. on Aerospace and Electronic Systems*, AES-16 (1), 23-52, (1980).

[20] William J. Caputi, Jr., “Stretch: A Time-Transformation Technique”, *IEEE Transactions on Aerospace and Electronic Systems*, Vol. AES-7, No. 2, pp 269-278, March 1971.

“The rule is perfect: in all matters of opinion our adversaries are insane.”

Mark Twain

DISTRIBUTION

Unlimited Release

1	MS 1330	S. C. Holswade	5340
1	MS 1330	B. L. Burns	5340
1	MS 0503	T. J. Mirabal	5341
1	MS 1330	J. G. Baldwin	5341
1	MS 1330	J. C. Lyle	5341
1	MS 1330	W. H. Hensley	5342
1	MS 1330	T. P. Bielek	5342
1	MS 1330	A. W. Doerry	5342
1	MS 1330	D. W. Harmony	5342
1	MS 1330	J. A. Hollowell	5342
1	MS 1330	S. S. Kawka	5342
1	MS 1330	M. S. Murray	5342
1	MS 0519	B. G. Rush	5342
1	MS 1330	D. G. Thompson	5342
1	MS 1330	K. W. Sorensen	5345
1	MS 1330	J. A. Bach	5345
1	MS 1330	D. F. Dubbert	5345
1	MS 1330	G. R. Sloan	5345
1	MS 0519	L. M. Wells	5354
1	MS 0519	D. L. Bickel	5354
1	MS 0519	J. T. Cordaro	5354
1	MS 0519	J. M. DeLaurentis	5354
1	MS 1330	S. M. Becker	5348
1	MS 1330	P. A. Dudley	5348
1	MS 1330	P. G. Ortiz	5348
1	MS 1330	D. C. Sprauer	5348
1	MS 1330	B. L. Tise	5348
2	MS 9018	Central Technical Files	8944
2	MS 0899	Technical Library	4536